State of the Global Climate 2020

WEATHER CLIMATE WATER

WORLD METEOROLOGICAL ORGANIZATION

WMO-No. 1264

WMO-No. 1264

Chair, Publications Board
World Meteorological Organization (WMO)
7 bis, avenue de la Paix
P.O. Box 2300
CH-1211 Geneva 2, Switzerland

Tel.: +41 (0) 22 730 84 03
Fax: +41 (0) 22 730 81 17
Email: publications@wmo.int

ISBN 978-92-63-11264-4

Cover illustration: Central photo: Dry grass wildfire caused by arson started a larch forest fire near Srednekolymsk, Sakha Republic, Russia, 24 June 2020. Contains modified Copernicus Sentinel data 2020. Photo credits: Pierre Markuse

Contents

Since 2016, the following United Nations agencies have significantly contributed to the WMO State of the Global Climate publication in support of climate policy and action:

Food and Agriculture Organization of the United Nations (FAO),

Intergovernmental Oceanographic Commission of the United Nations Educational, Scientific and Cultural Organization (IOC-UNESCO),

International Monetary Fund (IMF),

International Organization for Migration (IOM),

Office of the United Nations High Commissioner for Refugees (UNHCR),

United Nations Environment Programme (UNEP),

World Food Programme (WFP),

World Health Organization (WHO).

WMO also recognizes the substantial contributions that many non-United Nations organizations have made to this report. For a list of all the contributors to this report, see List of contributors.

Foreword

It has been 28 years since the World Meteorological Organization issued the first state of the climate report in 1993. The report was initiated due to the concerns raised at that time about projected climate change. While understanding of the climate system and computing power have increased since then, the basic message remains the same, and we now have 28 more years of data that show significant temperature increases over land and sea, as well as other changes, such as sea-level rise, melting of sea ice and glaciers and changes in precipitation patterns.

This underscores the robustness of climate science based on the physical laws governing the behaviour of the climate system. All key climate indicators and impact information provided in this report show relentless, continuing climate change, an increasing occurrence and intensification of high-impact events and severe losses and damages affecting people, societies and economies.

Concentrations of the major greenhouse gases continued to increase in 2019 and 2020. Globally averaged mole fractions of carbon dioxide (CO_2) have already exceeded 410 parts per million (ppm), and if the CO_2 concentration follows the same pattern as in previous years, it could reach or exceed 414 ppm in 2021.

Stabilizing global mean temperature at 1.5 °C to 2 °C above pre-industrial levels by the end of this century will require an ambitious reduction of greenhouse gas emissions, which must begin to occur during this decade.

I take this opportunity to congratulate the experts and the lead author, who compiled this report using physical data analyses and impact assessments. I thank all the contributors, particularly WMO Member National Meteorological and Hydrological Services and Regional Climate Centres and our sister United Nations Agencies for their collaboration and input on this report. The report is intended to help our organizations to update world leaders and citizens on the latest information about our Earth system's behaviour and climate change impacts. WMO remains committed to supporting this publication and communicating it widely for this purpose.

(P. Taalas)
Secretary-General

Foreword by the United Nations Secretary-General

2020 was an unprecedented year for people and planet: a global pandemic on a scale not seen for more than a century; global temperatures higher than in a millennium; and the highest concentration of carbon dioxide in our atmosphere for over 3 million years.

While many will remember 2020 most poignantly for how the COVID-19 pandemic affected the world, this report explains that, for many across the planet, especially in developing countries, 2020 was also a year of extreme weather and climate disruption, fuelled by anthropogenic climate change, affecting lives, destroying livelihoods and forcing many millions from their homes.

This report also demonstrates the impact of this warming, both on the planet's ecosystems and on individuals and communities, through superstorms, flooding, heatwaves, droughts and wildfires. We know what needs to be done to cut emissions and adapt to climate impacts now and in the future. We have the technology to succeed. But current levels of climate ambition and action are significantly short of what is needed.

We know that to avert the worst impacts of climate change, we must keep global temperatures to within 1.5 °C of the pre-industrial baseline. That means reducing global greenhouse gas emissions by 45 per cent from 2010 levels by 2030 and reaching net zero emissions by 2050. The data in this report show that the global mean temperature for 2020 was around 1.2 °C warmer than pre-industrial times, meaning that time is fast running out to meet the goals of the Paris Agreement. We need to do more, and faster, now.

This year is pivotal. At the United Nations climate conference, COP26, in November, we need to demonstrate that we are taking and planning bold action on mitigation and adaptation. This entails scaled-up financial flows from developed to developing countries. And it means radical changes in all financial institutions, public and private, to ensure that they fund sustainable and resilient development for all and move away from a grey and inequitable economy.

As the world focuses on COVID-19 recovery, let us use the opportunity to get back on track to achieve the Sustainable Development Goals and reduce the threat from climate change. I call on everyone – from governments, civil society and business to individual citizens – to work to make 2021 count.

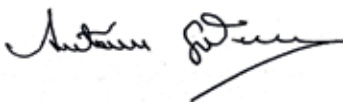

(A. Guterres)
United Nations Secretary-General

Highlights

Concentrations of the major greenhouse gases, CO_2, CH_4, and N_2O, continued to increase despite the temporary reduction in emissions in 2020 related to measures taken in response to COVID-19.

2020 was one of the three warmest years on record. The past six years, including 2020, have been the six warmest years on record. Temperatures reached 38.0 °C at Verkhoyansk, Russian Federation on 20 June, the highest recorded temperature anywhere north of the Arctic Circle.

The trend in sea-level rise is accelerating. In addition, ocean heat storage and acidification are increasing, diminishing the ocean's capacity to moderate climate change.

The Arctic minimum sea-ice extent in September 2020 was the second lowest on record. The sea-ice retreat in the Laptev Sea was the earliest observed in the satellite era.

The Antarctic mass loss trend accelerated around 2005, and currently, Antarctica loses approximately 175 to 225 Gt of ice per year.

The 2020 North Atlantic hurricane season was exceptionally active. Hurricanes, extreme heatwaves, severe droughts and wildfires led to tens of billions of US dollars in economic losses and many deaths.

Some 9.8 million displacements, largely due to hydrometeorological hazards and disasters, were recorded during the first half of 2020.

Disruptions to the agriculture sector by COVID-19 exacerbated weather impacts along the entire food supply chain, elevating levels of food insecurity.

Global climate indicators

Global climate indicators[1] reveal the ways in which the climate is changing and provide a broad view of the climate at the global scale. They are used to monitor the key components of the climate system and describe the most relevant changes in the composition of the atmosphere, the heat that arises from the accumulation of greenhouse gases (and other factors), and the responses of the land, ocean and ice to the changing climate. These indicators include global mean surface temperature, global ocean heat content, state of ocean acidification, glacier mass balance, Arctic and Antarctic sea-ice extent, global CO_2 mole fraction and global mean sea level and are discussed in detail in the sections below. Further information on the data sets used for each indicator can be found at the end of this report.

A variety of baselines are used in this report. For global mean temperature, the baseline is 1850–1900, which is the baseline used in the IPCC Special Report on Global Warming of 1.5 °C as an approximation of pre-industrial temperatures.[2] For greenhouse gases, pre-industrial concentrations estimated from ice cores for the year 1750 are used as baselines.

For other variables and for temperature maps, the WMO climatological standard normal 1981–2010 is used, where possible, as a base period for consistent reporting of surface measurements, satellite data and reanalyses. For some indicators, it is not possible to use this base period, either because there are no measurements in the early part of the period, or because a longer base period is needed to calculate a representative average. Where the base period used is different from 1981–2010, this is noted in the text or figure captions, and more details are given in the Data set details section.

TEMPERATURE

The global mean temperature for 2020 was 1.2 ± 0.1 °C above the 1850–1900 baseline (Figure 1), which places 2020 as one of the three warmest years on record globally. The WMO assessment is based on five global temperature data sets (Figure 1). All five of these data sets currently place 2020 as one of the three warmest years on record. The spread of the five estimates of the annual global mean ranges between 1.15 °C and 1.28 °C above pre-industrial levels (see the baseline definition in the Global climate indicators section). It is worth noting that the Paris Agreement aims to hold the global average temperature to well below 2 °C above

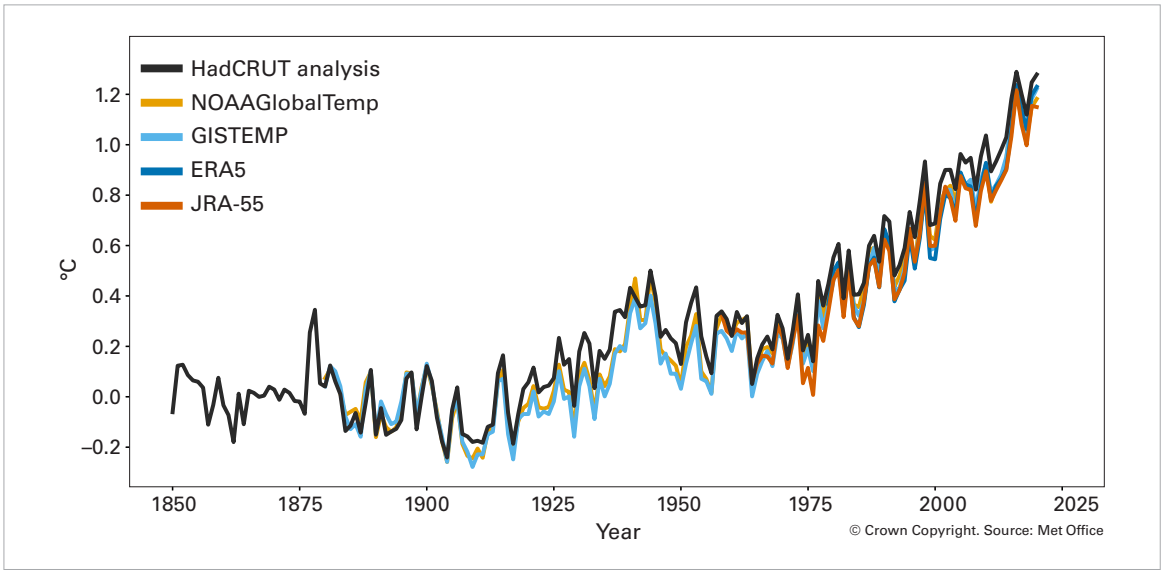

Figure 1. Global annual mean temperature difference from pre-industrial conditions (1850–1900) for five global temperature data sets. For details of the data sets and plotting, see Temperature data in the Data set details section at the end of this report.

[1] https://journals.ametsoc.org/view/journals/bams/aop/bamsD190196/bamsD190196.xml

[2] http://www.ipcc.ch/sr15/

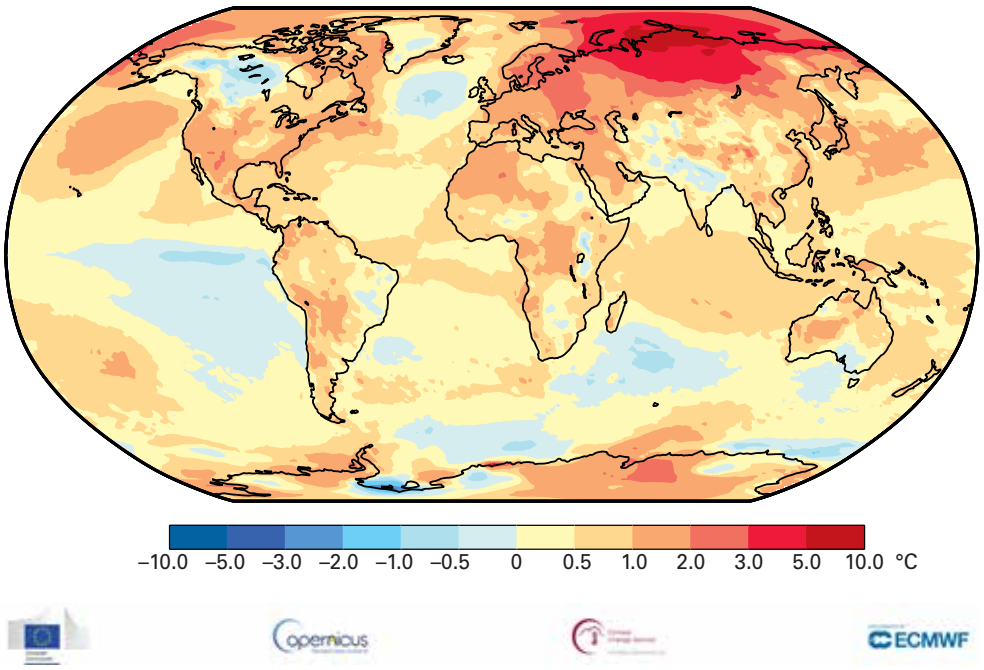

Figure 2. Temperature anomalies relative to the 1981–2010 long-term average from the ERA5 reanalysis for 2020. *Source:* Copernicus Climate Change Service, European Centre for Medium-Range Weather Forecasts (ECMWF)

pre-industrial levels and to pursue efforts to limit the temperature increase to 1.5 °C above pre-industrial levels[3]. Assessing the increase in global temperature in the context of climate change refers to the long-term global average temperature, not to the averages for individual years or months.

The warmest year on record to date, 2016, began with an exceptionally strong El Niño, a phenomenon which contributes to elevated global temperatures. Despite neutral or comparatively weak El Niño conditions early in 2020[4] and La Niña conditions developing by late September,[5] the warmth of 2020 was comparable to that of 2016.

With 2020 being one of the three warmest years on record, the past six years, 2015–2020, were the six warmest on record. The last five-year (2016–2020) and 10-year (2011–2020) averages were also the warmest on record.

Although the overall warmth of 2020 is clear, there were variations in temperature anomalies across the globe (Figure 2). While most land areas were warmer than the long-term average (1981–2010), one area in northern Eurasia stands out with temperatures of more than five degrees above average (see The Arctic in 2020). Other notable areas of warmth included limited areas of the south-western United States, the northern and western parts of South America, parts of Central America, and wider areas of Eurasia, including parts of China. For Europe, 2020 was the warmest year on record. Areas of below-average temperatures on land included western Canada, limited areas of Brazil, northern India, and south-eastern Australia.

Over the ocean, unusual warmth was observed in parts of the tropical Atlantic and Indian Oceans. The pattern of sea-surface temperature anomalies in the Pacific is characteristic of La Niña, having cooler-than-average surface waters in the eastern equatorial Pacific surrounded by a horseshoe-shaped band of warmer-than-average waters, most notably in the North-East Pacific and along the western edge of the Pacific from Japan to Papua New Guinea.

[3] https://unfccc.int/process-and-meetings/the-paris-agreement/the-paris-agreement

[4] https://origin.cpc.ncep.noaa.gov/products/analysis_monitoring/ensostuff/ONI_v5.php

[5] http://www.bom.gov.au/climate/enso/wrap-up/archive/20200929.archive.shtml

GREENHOUSE GASES AND STRATOSPHERIC OZONE

GREENHOUSE GASES

Atmospheric concentrations of greenhouse gases reflect a balance between emissions from human activities and natural sources, and sinks in the biosphere and ocean. Increasing levels of greenhouse gases in the atmosphere due to human activities have been the major driver of climate change since the mid-twentieth century. Global average mole fractions of greenhouse gases are calculated from in situ observations made at multiple sites in the Global Atmosphere Watch Programme of WMO and partner networks.

In 2019, greenhouse gas concentrations reached new highs (Figure 3), with globally averaged mole fractions of carbon dioxide (CO_2) at 410.5 ± 0.2 parts per million (ppm), methane (CH_4) at 1 877 ± 2 parts per billion (ppb) and nitrous oxide (N_2O) at 332.0 ± 0.1 ppb, respectively, 148%, 260% and 123% of pre-industrial (before 1750) levels. The increase in CO_2 from 2018 to 2019 (2.6 ppm) was larger than both the increase from 2017 to 2018 (2.3 ppm) and the average yearly increase over the last decade (2.37 ppm per year). For CH_4, the increase from 2018 to 2019 was slightly lower than the increase from 2017 to 2018 but still higher than the average yearly increase over the last decade. For N_2O, the increase from 2018 to 2019 was also lower than that observed from 2017 to 2018 and close to the average growth rate over the past 10 years.

The temporary reduction in emissions in 2020 related to measures taken in response to COVID-19[6] is likely to lead to only a slight decrease in the annual growth rate of CO_2 concentration in the atmosphere, which will be practically indistinguishable from the natural interannual variability driven largely by the terrestrial biosphere. Real-time data from specific locations, including Mauna Loa (Hawaii) and Cape Grim (Tasmania) indicate that levels of CO_2, CH_4 and N_2O continued to increase in 2020.

The IPCC Special Report on Global Warming of 1.5 °C found that limiting warming to 1.5 °C

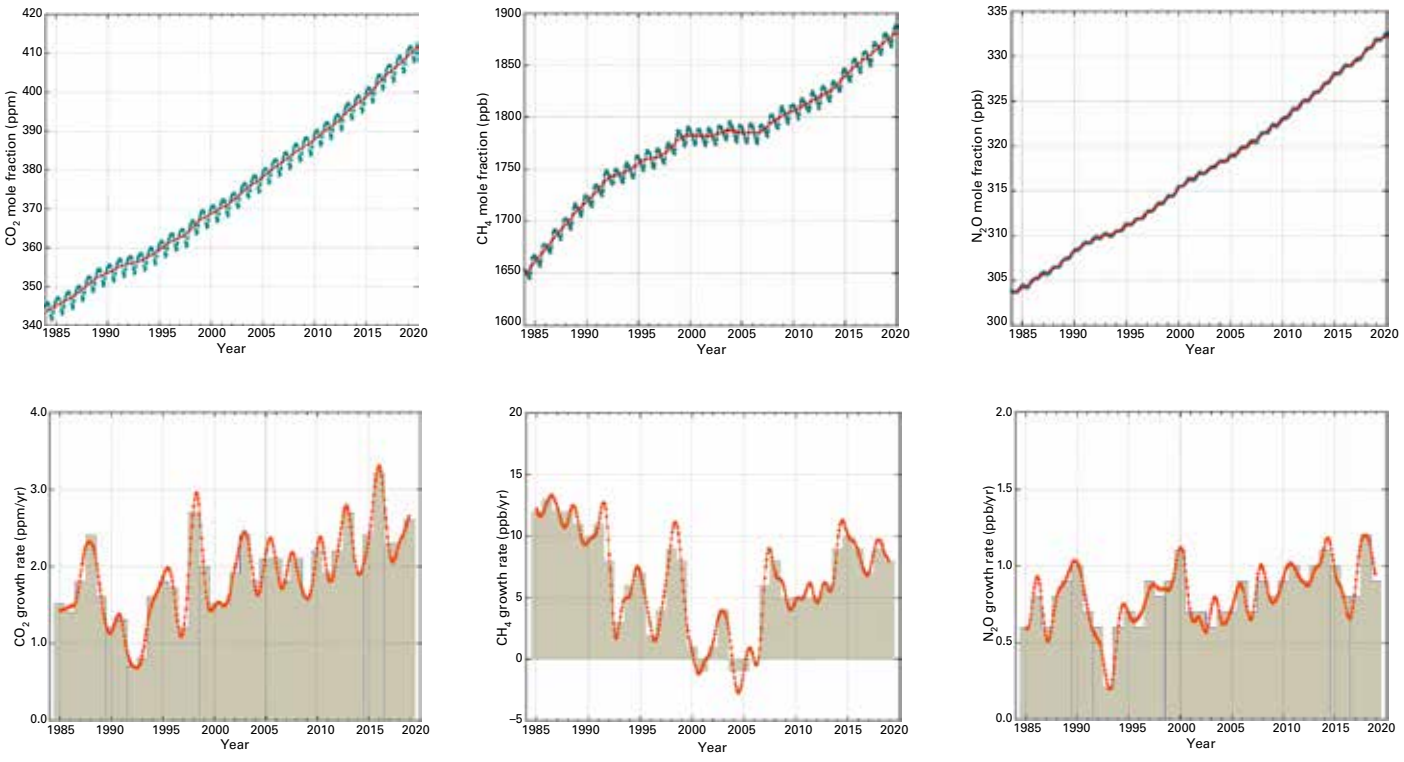

Figure 3. Top row: Globally averaged mole fraction (measure of concentration), from 1984 to 2019, of CO_2 in parts per million (left), CH_4 in parts per billion (centre) and N_2O in parts per billion (right). The red line is the monthly mean mole fraction with the seasonal variations removed; the blue dots and line show the monthly averages. Bottom row: The growth rates representing increases in successive annual means of mole fractions are shown as grey columns for CO_2 in parts per million per year (left), CH_4 in parts per billion per year (centre) and N_2O in parts per billion per year (right).
Source: WMO Global Atmosphere Watch

[6] Liu, Z. et al., 2020: Near-real-time monitoring of global CO_2 emissions reveals the effects of the COVID-19 pandemic. *Nature Communications*, 11(1): 5172, https://doi.org/10.1038/s41467-020-18922-7.

above pre-industrial levels implies reaching net zero CO_2 emissions globally by around 2050, with concurrent deep reductions in emissions of non-CO_2 forcers.

STRATOSPHERIC OZONE AND OZONE-DEPLETING GASES

Following the success of the Montreal Protocol, the use of halons and chlorofluorocarbons has been reported as discontinued, but their levels in the atmosphere continue to be monitored. Because of their long lifetime, these compounds will remain in the atmosphere for many decades, and even if there are no new emissions, there is still more than enough chlorine and bromine present in the atmosphere to cause the complete destruction of ozone in Antarctica from August to December. As a result, the formation of the Antarctic ozone hole continues to be an annual spring event, with the year-to-year variation in its size and depth governed to a large degree by meteorological conditions.

The 2020 Antarctic ozone hole developed early and went on to be the longest-lasting and one of the deepest ozone holes since ozone layer monitoring began 40 years ago (Figure 4). The ozone hole area reached its maximum area for 2020 on 20 September at 24.8 million km^2, the same area as was reached in 2018. The area of the hole was closer to the maxima observed in 2015 (28.2 million km^2) and 2006 (29.6 million km^2) than the maximum that was reached in 2019 (16.4 million km^2) according to an analysis from the National Aeronautics and Space Administration (NASA). The unusually deep and long-lived ozone hole was driven by a strong and stable polar vortex and very low temperatures in the stratosphere.

At the other end of the Earth, unusual atmospheric conditions also led to ozone concentrations over the Arctic falling to a record low for the month of March. Unusually weak "wave" events in the upper atmosphere left the polar vortex relatively undisturbed, preventing the mixing of ozone-rich air from lower latitudes. In addition, early in the year, the stratospheric polar vortex over the Arctic was strong, and this, combined with consistently very low temperatures, allowed a large area of polar stratospheric clouds to grow. When the sun rises after the polar winter, it triggers chemical processes in the polar stratospheric clouds that lead to the depletion of ozone. Measurements from weather balloons indicated that ozone depletion surpassed the levels reported in 2011 and, together with satellite observations, documented stratospheric ozone levels of approximately 205 Dobson Units on 12 March 2020. The typical lowest ozone values previously observed over the Arctic in March are at least 240 Dobson Units.

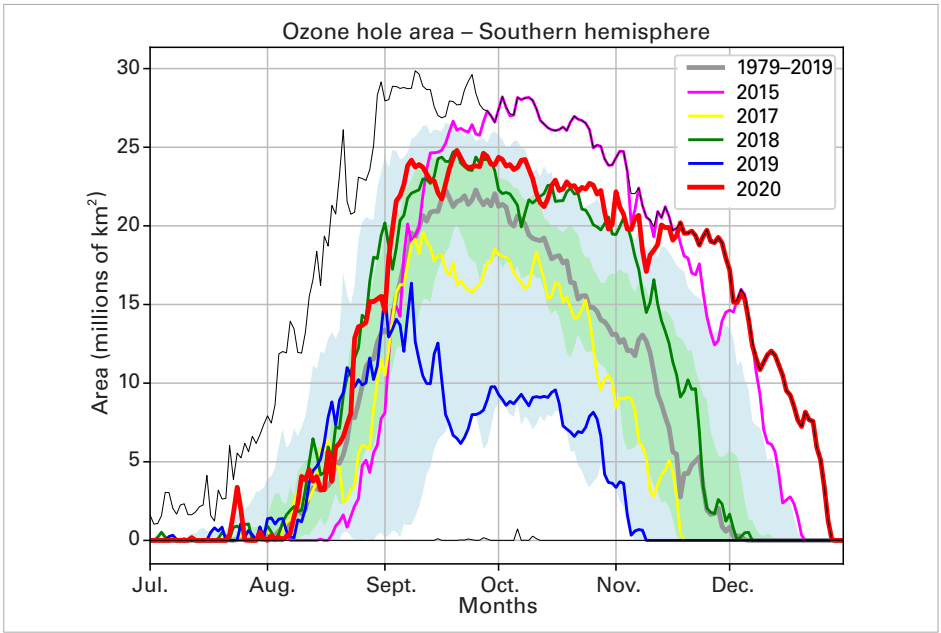

Figure 4. Area (millions of km^2) where the total ozone column is less than 220 Dobson units. 2020 is shown in red, and the most recent years are shown for comparison as indicated by the legend. The thick grey line is the 1979–2019 average. The blue shaded area represents the 30th to 70th percentiles, and the green shaded area represents the 10th and 90th percentiles for the period 1979–2019. The thin black lines show the maximum and minimum values for each day in the 1979–2019 period. The plot was made at WMO on the basis of data downloaded from NASA Ozone Watch (https://ozonewatch.gsfc.nasa.gov/). The NASA data are based on satellite observations from the OMI and TOMS instruments.

OCEAN

The majority of the excess energy that accumulates in the Earth system due to increasing concentrations of greenhouse gases is taken up by the ocean. The added energy warms the ocean, and the consequent thermal expansion of the water leads to sea-level rise, which is further increased by melting ice. The surface of the ocean warms more rapidly than the interior, and this can be seen in the rise of the global mean temperature and in the increased incidence of marine heatwaves. As the concentration of CO_2 in the atmosphere rises, so too does the concentration of CO_2 in the oceans. This affects ocean chemistry, lowering the average pH of the water, a process known as ocean acidification. All these changes have a broad range of impacts in the open ocean and coastal areas.

OCEAN HEAT CONTENT

Increasing human emissions of CO_2 and other greenhouse gases cause a positive radiative imbalance at the top of the atmosphere – the Earth Energy Imbalance (EEI) – which is driving global warming through an accumulation of energy in the form of heat in the Earth system.[7,8,9] Ocean heat content (OHC) is a measure of this heat accumulation in the Earth system as around 90% of it is stored in the ocean. A positive EEI signals that the Earth's climate system is still responding to the current forcing[10] and that more warming will occur even if the forcing does not increase further.[11]

Historical measurements of subsurface temperature back to the 1940s mostly rely on shipboard measurement systems, which constrain the availability of subsurface temperature observations at the global scale and at depth.[12] With the deployment of the Argo network of autonomous profiling floats, which first achieved near-global coverage in 2006, it is now possible to routinely measure OHC changes to a depth of 2000 m.[13,14]

Various research groups have developed estimates of global OHC. Although they all rely more or less on the same database, the estimates show differences arising from the various statistical treatments of data gaps, the choice of climatology and the approach used to account for instrumental biases.[9,15] A concerted effort has been established to provide an international assessment on the global evolution of ocean warming,[16] and an

---

[7] Hansen, J. et al., 2005: Earth's Energy Imbalance: Confirmation and Implications. *Science,* 308(5727): 1431–1435, https://doi.org/10.1126/science.1110252.

[8] Intergovernmental Panel on Climate Change, 2013: *Climate change 2013: The Physical Science Basis*, https://www.ipcc.ch/report/ar5/wg1/.

[9] von Schuckmann, K. et al., 2016: An imperative to monitor Earth's energy imbalance. *Nature Climate Change,* 6(2): 138–144, https://doi.org/10.1038/nclimate2876.

[10] Hansen, J. et al., 2011: EEarth's energy imbalance and implications. *Atmospheric Chemistry and Physics*, 11(24): 13421–13449, https://doi.org/10.5194/acp-11-13421-2011.

[11] Hansen, J. et al., 2017: Young people's burden: requirement of negative CO_2 emissions. *Earth System Dynamics*, 8(3): 577–616, https://doi.org/10.5194/esd-8-577-2017.

[12] Abraham, J.P. et al., 2013: A review of global ocean temperature observations: Implications for ocean heat content estimates and climate change. *Reviews of Geophysics*, 51(3): 450–483, https://doi.org/10.1002/rog.20022.

[13] Riser, S.C. et al., 2016: Fifteen years of ocean observations with the global Argo array. *Nature Climate Change*, 6(2): 145–153, https://doi.org/10.1038/nclimate2872.

[14] Roemmich, D. et al., 2019: On the Future of Argo: A Global, Full-Depth, Multi-Disciplinary Array. *Frontiers in Marine Science*, 6, https://doi.org/10.3389/fmars.2019.00439.

[15] Boyer, T. et al., 2016: Sensitivity of Global Upper-Ocean Heat Content Estimates to Mapping Methods, XBT Bias Corrections, and Baseline Climatologies. *Journal of Climate*, 29(13): 4817–4842, https://doi.org/10.1175/JCLI-D-15-0801.1.

[16] von Schuckmann, K. et al., 2020: Heat stored in the Earth system: where does the energy go? *Earth System Science Data*, 12(3): 2013–2041, https://doi.org/10.5194/essd-12-2013-2020.

update of the entire analysis to 2019 is shown in Figure 5 and Figure 6.

The 0–2 000 m depth layer of the global ocean continued to warm in 2019, reaching a new record high (Figure 5), and it is expected that it will continue to warm in the future.[17] A preliminary analysis based on three global data sets suggests that 2020 exceeded that record. Heat storage at intermediate depth (700–2 000 m) increased at a comparable rate to the rate of heat storage in the 0–300 m depth layer, which is in general agreement with the 15 international OHC estimates (Figure 6). All data sets agree that ocean warming rates show a particularly strong increase over the past two decades. Moreover, there is a clear indication that

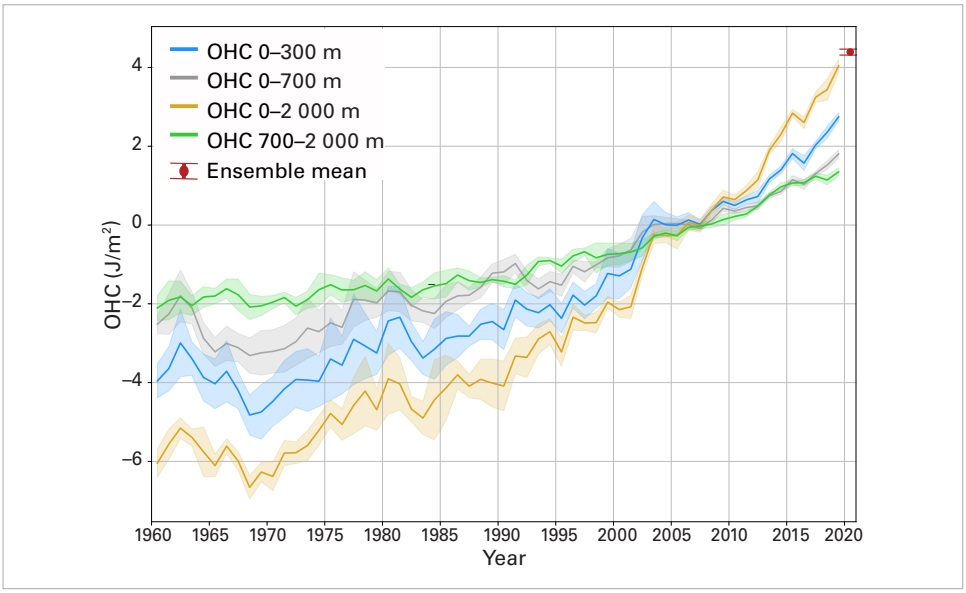

Figure 5. 1960–2019 ensemble mean time series and ensemble standard deviation (2-sigma, shaded) of global OHC anomalies relative to the 2005–2017 climatology. The ensemble mean is an outcome of a concerted international effort, and all products used are listed in Ocean heat content data and in the legend of Figure 5. Note that values are given for the ocean surface area between 60°S–60°N and limited to the 300 m bathymetry of each product.
Source: Updated from von Schuckmann, K. et al., 2016 (see footnote 9). The ensemble mean OHC (0–2 000 m) anomaly (relative to the 1993–2020 climatology) has been added as a red point, together with its ensemble spread, and is based on Copernicus Marine Environment Monitoring Service (CMEMS) (Coriolis Ocean Dataset for Reanalysis (CORA)) products (see Cheng et al., 2017 and Ishii et al., 2017 in Ocean heat content data).

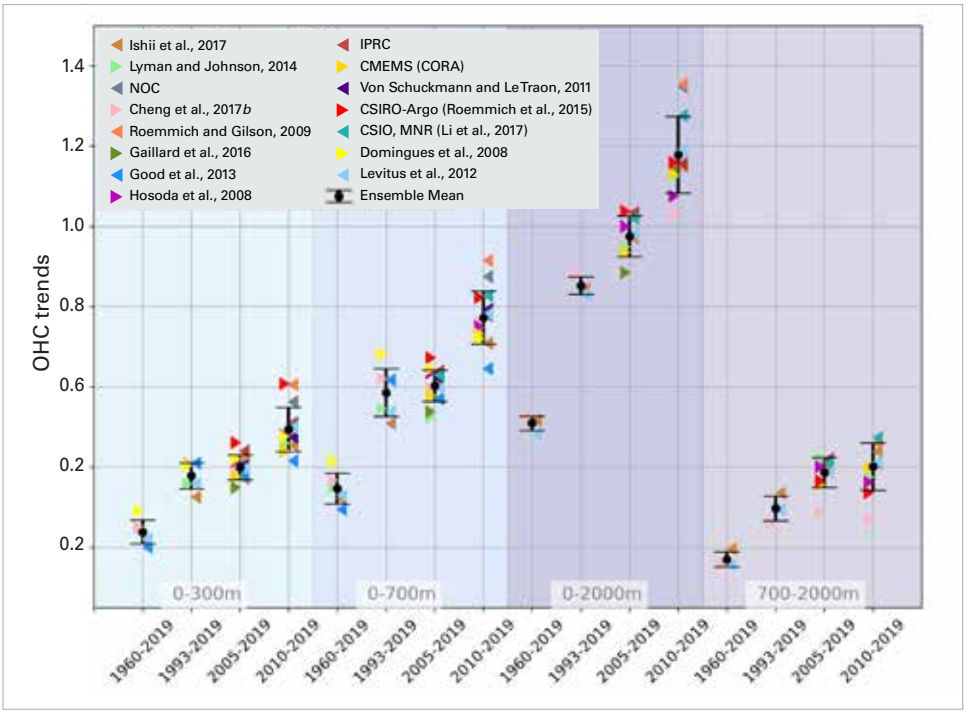

Figure 6. Linear trends of global OHC as derived from different temperature products (colours). References are listed in Ocean heat content data. The ensemble mean and standard deviation (2-sigma) is given in black. The shaded areas show trends from different depth layer integrations: 0–300 m (light turquoise), 0–700 m (light blue), 0–2 000 m (purple) and 700–2 000 m (light purple). For each integration depth layer, trends are evaluated over four periods: historical (1960–2019), altimeter era (1993–2019), golden Argo era (2005–2019), and the most recent period of 2010–2019.
Source: Updated from von Schuckmann, K. et al., 2016 (see footnote 9).

[17] Intergovernmental Panel on Climate Change, 2019: *IPCC Special Report on the Ocean and Cryosphere in a Changing Climate*, https://www.ipcc.ch/srocc/.

heat sequestration into the ocean below 700 m depth has occurred over the past six decades and is linked to an increase in OHC trends over time. Ocean warming rates for the 0–2 000 m depth layer reached rates of 1.2 (0.8) ± 0.2 Wm^{-2} over the period 2010–2019. Below 2 000 m depth, the ocean also warmed, albeit at the lower rate of 0.07 ± 0.04 Wm^{-2} from 1991 to 2018.[18]

SEA LEVEL

On average, since early 1993, the altimetry-based global mean rate of sea-level rise has amounted to 3.3 ± 0.3 mm/yr. The rate has also increased over that time. A greater loss of ice mass from the ice sheets is the main cause of the accelerated rise in global mean sea level.[19]

Global mean sea level continued to rise in 2020 (Figure 7, left). A small decrease during the northern hemisphere summer was likely related to La Niña conditions in the tropical Pacific. Interannual changes of global mean sea level around the long-term trend are correlated with El Niño–Southern Oscillation (ENSO) variability (Figure 7, right). During La Niña events, such as that which occurred in late 2020 and the strong La Niña of 2011, shifts in rainfall patterns transfer water mass from the ocean to tropical river basins on land, temporarily reducing global mean sea level. The opposite is observed during El Niño (for example, the strong 2015/2016 El Niño). In 2020, exceptional rainfall across the African Sahel and other regions may also have contributed to a temporary slowing in sea-level rise as flood waters slowly found their way back to the sea. However, by the end of 2020, global mean sea level was rising again.

At the regional scale, sea level continues to rise non-uniformly. The strongest regional trends over the period from January 1993 to June 2020 were seen in the southern hemisphere: east of Madagascar in the Indian Ocean; east of New Zealand in the Pacific Ocean; and east of Rio de la Plata/South America in the South Atlantic Ocean. An elongated eastward pattern was also seen in the North Pacific Ocean. The strong pattern that was seen in the western tropical Pacific Ocean over the first two decades of the altimetry record is now fading, suggesting that it was related to short-term variability. Regional sea-level trends are dominated by variations in ocean heat content.[17] However, in some regions, such as the Arctic, salinity changes due to freshwater input from the melting of ice on land play an important role.

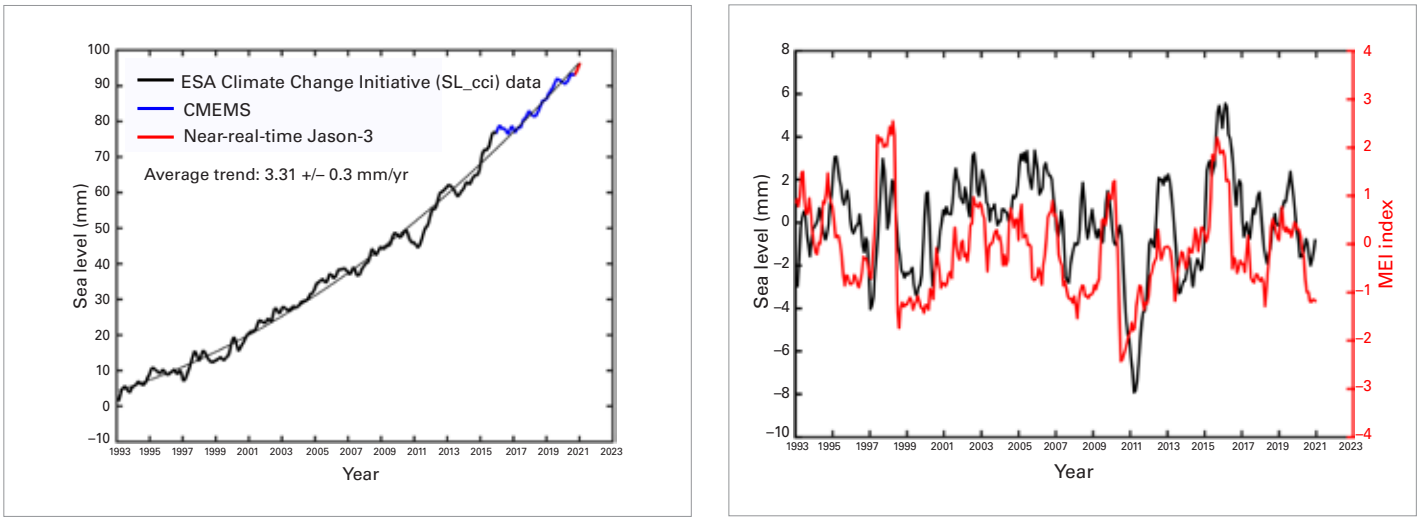

Figure 7. Left: Satellite altimetry-based global mean sea level for January 1993 to January 2021 (last data: 21 January 2021). Data from the European Space Agency Climate Change Initiative Sea Level project (January 1993 to December 2015, thick black curve), data from CMEMS (January 2016 to November 2020, blue curve) and near-real-time altimetry data from the Jason-3 mission beyond November 2020 (red curve). The thin black curve is a quadratic function that best fits the data. Right: Interannual variability of the global mean sea level (with the quadratic function shown in the left-hand panel subtracted) (black curve and left axis) with the multivariate ENSO index (MEI) (red curve and right axis).

[18] Update from Purkey, S.G. and G.C. Johnson, 2010: Warming of Global Abyssal and Deep Southern Ocean Waters between the 1990s and 2000s: Contributions to Global Heat and Sea Level Rise Budgets. *Journal of Climate*, 23(23): 6336–6351, https://doi.org/10.1175/2010JCLI3682.1.

[19] WCRP Global Sea Level Budget Group, 2018: Global sea-level budget 1993–present. *Earth System Science Data*, 10(3): 1551–1590, https://doi.org/10.5194/essd-10-1551-2018.

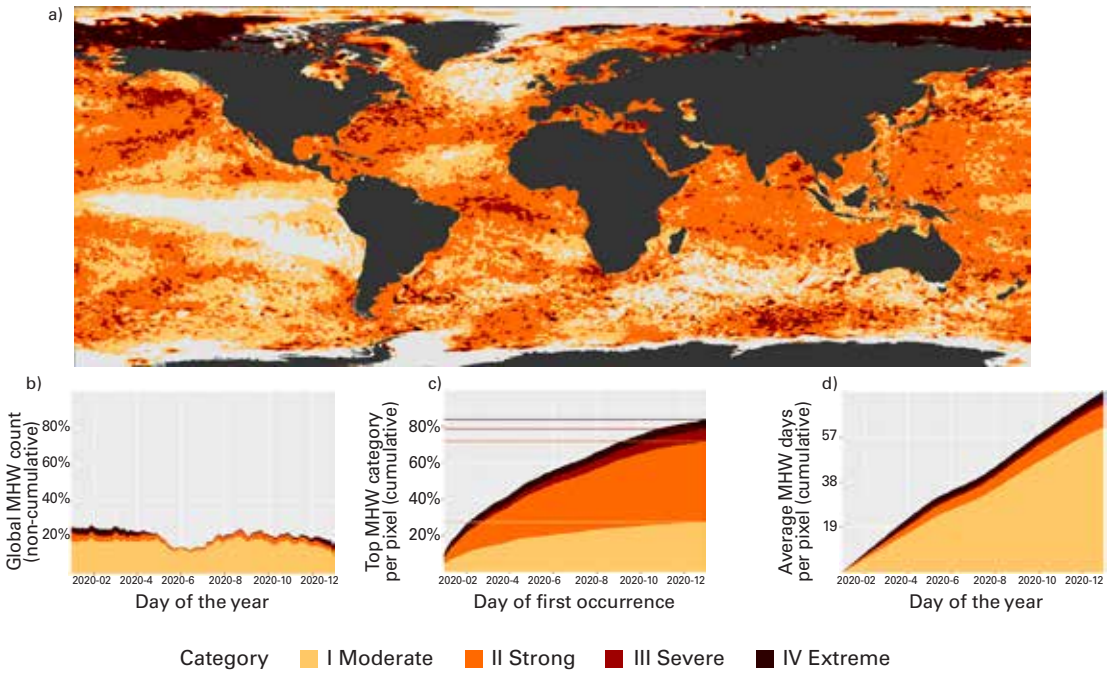

Figure 8. (a) Global map showing the highest MHW category (for definitions, see Marine heatwave data) experienced at each pixel over the course of the year (reference period 1982–2011). Light grey indicates that no MHW occurred in a pixel over the entire year; (b) Stacked bar plot showing the percentage of ocean pixels experiencing an MHW on any given day of the year; (c) Stacked bar plot showing the cumulative percentage of the ocean that experienced an MHW over the year. Note: These values are based on when in the year a pixel first experienced its highest MHW category, so no pixel was counted more than once. Horizontal lines in this figure show the final percentages for each category of MHW; (d) Stacked bar plot showing the cumulative number of MHW days averaged over all pixels in the ocean. Note: This average is calculated by dividing the cumulative number of MHW days per pixel for the entire ocean by the overall number of ocean pixels (~690 000). *Source:* Robert Schlegel

MARINE HEATWAVES

As with heatwaves on land, extreme heat can affect the near-surface layer of the oceans. This situation is called a marine heatwave (MHW), and it can cause a range of consequences for marine life and dependent communities. Satellite retrievals of sea-surface temperature can be used to monitor MHWs. An MHW is categorized here as moderate, strong, severe or extreme (for definitions, see Marine heatwave data).

Much of the ocean experienced at least one 'strong' MHW at some point in 2020 (Figure 8a). Conspicuously absent are MHWs in the Atlantic Ocean south of Greenland and in the eastern equatorial Pacific Ocean. The Laptev Sea experienced a particularly intense MHW from June to December. Sea-ice extent was unusually low in that region, and adjacent land areas experienced heatwaves during the summer (see The Arctic in 2020). Another important MHW to note in 2020 was the return of the semi-persistent warm region in the North-East Pacific Ocean. This event is similar in scale to the original 'blob',[20,21] which developed around 2013, with remnants lasting until 2016.[22] Approximately one fifth of the global ocean was experiencing an MHW on any given day in 2020 (Figure 8b). This percentage is similar to that of 2019, but less than the 2016 peak percentage of 23%. More of the ocean experienced MHWs classified as 'strong' (45%) than 'moderate' (28%). In total, 84% of the ocean experienced at least one MHW during 2020 (Figure 8c); this is similar to the percentage of the ocean that experienced MHWs in 2019 (also 84%), but below the 2016 peak (88%).

[20] Gentemann, C.L. et al., 2017: Satellite sea surface temperatures along the West Coast of the United States during the 2014–2016 northeast Pacific marine heat wave. *Geophysical Research Letters*, 44(1): 312–319, https://doi.org/10.1002/2016GL071039.

[21] di Lorenzo, E. and N. Mantua, 2016: Multi-Year Persistence of the 2014/15 North Pacific Marine Heatwave. *Nature Climate Change*, 6: 1042–1047, https://doi.org/10.1038/nclimate3082.

[22] Schmeisser, L. et al., 2019: The Role of Clouds and Surface Heat Fluxes in the Maintenance of the 2013–2016 Northeast Pacific Marine Heatwave. *Journal of Geophysical Research: Atmospheres*, 124(20): 10772–10783, https://doi.org/10.1029/2019JD030780.

OCEAN ACIDIFICATION

The ocean absorbs around 23% of the annual emissions of anthropogenic CO_2 into the atmosphere,[23] thereby helping to alleviate the impacts of climate change.[24] However, the CO_2 reacts with seawater, lowering its pH. This process, known as ocean acidification, affects many organisms and ecosystem services, threatening food security by endangering fisheries and aquaculture. This is particularly a problem in the polar oceans. It also affects coastal protection by weakening coral reefs, which shield coastlines. As the pH of the ocean declines, its capacity to absorb CO_2 from the atmosphere decreases, diminishing the ocean's capacity to moderate climate change. Regular global observations and measurements of ocean pH are needed to improve the understanding of the consequences of its variations, enable modelling and prediction of change and variability, and help inform mitigation and adaptation strategies.

Global efforts have been made to collect and compare ocean acidification observation data. These data contribute towards achieving Sustainable Development Goal (SDG) 14.3 and can be used to determine its associated SDG Indicator 14.3.1: "Average marine acidity (pH) measured at agreed suite of representative sampling stations". They are summarized in Figure 9 (left) and show an increase of variability (minimum and maximum pH values are highlighted) and a decline in average pH at the available observing sites between 2015 and 2019. The steady global change (Figure 9, right) estimated from a wide variety of sources, including measurements of other variables, contrasts with the regional and seasonal variations in ocean carbonate chemistry seen at individual sites. The increase in the amount of available data highlights the variability and the trend in ocean acidification, as well as the need for sustained long-term observations to better characterize the natural variability in ocean carbonate chemistry.

DEOXYGENATION

Since 1950, the open ocean oxygen content has decreased by 0.5–3%.[17] Oxygen minimum zones, which are permanent features of the open ocean, are expanding.[25] The trend of deoxygenation in the global coastal ocean is still uncertain. Since 1950, the number of hypoxic sites in the global coastal ocean has increased in response to worldwide eutrophication.[26] A quantitative assessment of the severity of

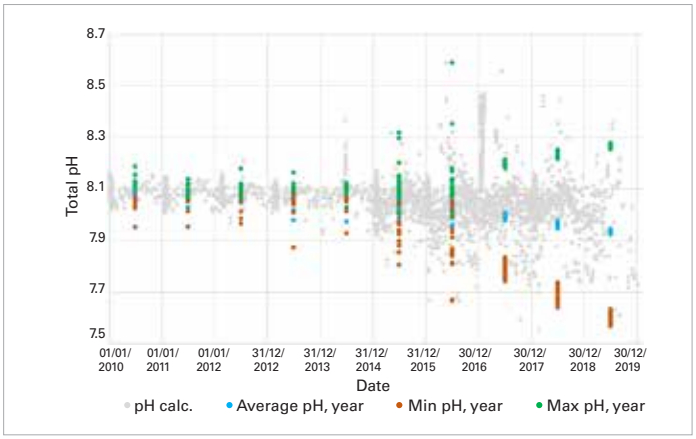

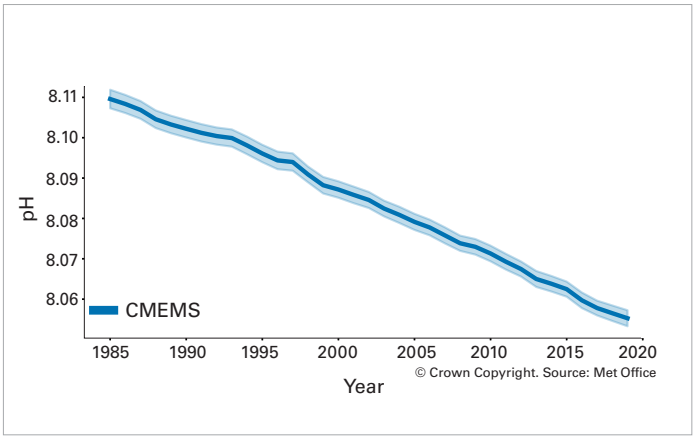

Figure 9. Left: Surface pH values based on ocean acidification data submitted to the 14.3.1 data portal (http://oa.iode.org) for the period from 1 January 2010 to 8 January 2020. The grey circles represent the calculated pH of data submissions (including all data sets with data for at least two carbonate parameters); the blue circles represent the average annual pH (based on data sets with data for at least two carbonate parameters); the red circles represent the annual minimum pH and the green circles represent the annual maximum pH. Note that the number of stations is not constant with time. Right: Global mean surface pH from E.U. Copernicus Marine Service Information (blue). The shaded area indicates the estimated uncertainty in each estimate.

[23] World Meteorological Organization, 2019: *WMO Greenhouse Gas Bulletin: The State of Greenhouse Gases in the Atmosphere Based on Global Observations through 2018*, No. 15, https://library.wmo.int/index.php?lvl=notice_display&id=21620.

[24] Friedlingstein, P. et al., 2020: Global Carbon Budget 2020. *Earth System Science Data*, 12(4): 3269–3340, https://doi.org/10.5194/essd-12-3269-2020.

[25] Breitburg, D.et al., 2018: Declining oxygen in the global ocean and coastal waters. *Science (New York, N.Y.)*, 359(6371), https://doi.org/10.1126/science.aam7240.

[26] Diaz, R.J. and R. Rosenberg, 2008: Spreading Dead Zones and Consequences for Marine Ecosystems. *Science*, 321(5891): 926–929, https://doi.org/10.1126/science.1156401.

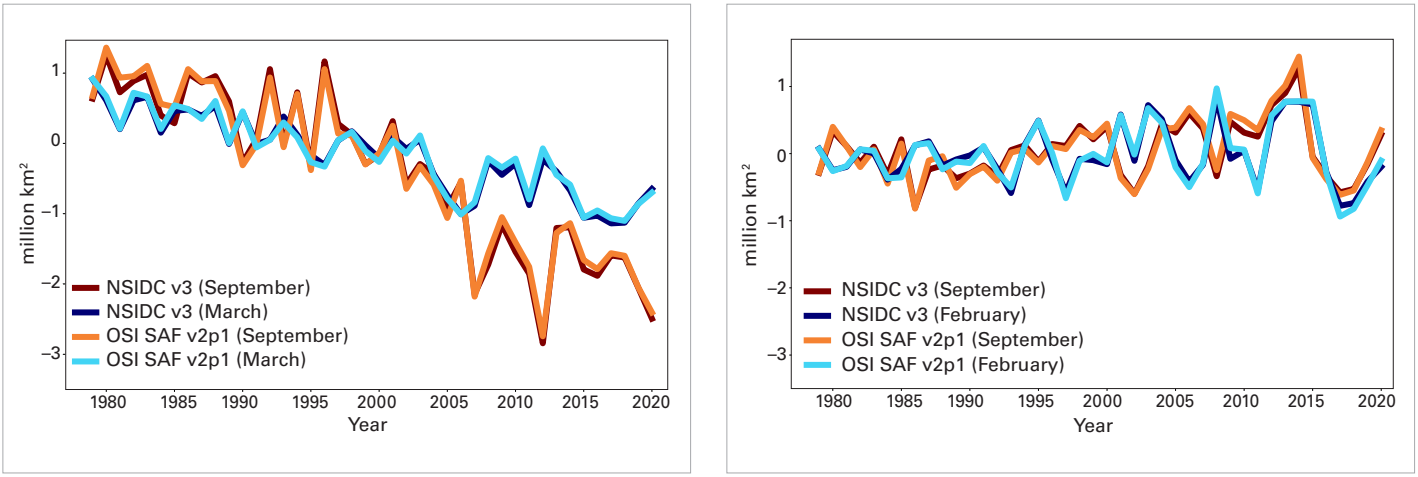

Figure 10. Sea-ice extent difference from the 1981–2010 average in the Arctic (left) and Antarctic (right) for the months with maximum ice cover (Arctic: March; Antarctic: September) and minimum ice cover (Arctic: September; Antarctic: February). *Source:* Data from EUMETSAT OSI SAF v2p1 (Lavergne et al., 2019) and National Snow and Ice Data Centre (NSIDC) v3 (Fetterer et al., 2017) (see reference details in Sea-ice data).

hypoxia on marine life at the global coastal scale requires characterizing the dynamics of hypoxia, for which there is currently insufficient data.

A comprehensive assessment of deoxygenation in the open and coastal ocean would benefit from building a consistent, quality-controlled, open-access global ocean oxygen data set and atlas complying with the FAIR[27] principles. An effort in this direction has been initiated by the Global Ocean Oxygen Network (GO_2NE), the International Ocean Carbon Coordination Project (IOCCP), the National Oceanic and Atmospheric Administration (NOAA) and the German Collaborative Research Centre 754 (SFB 754) project. This effort is part of the Global Ocean Oxygen Decade (GOOD) proposal submitted to the United Nations Decade of Ocean Sciences for Sustainable Development.

CRYOSPHERE

The cryosphere is the domain that comprises the frozen parts of the earth. The cryosphere provides key indicators of the changing climate, but it is one of the most under-sampled domains. The major cryosphere indicators used in this report are sea-ice extent, glacier mass balance and mass balance of the Greenland and Antarctic ice sheets. Specific snow events are covered in the High-impact events in 2020 section.

SEA ICE

In the Arctic, the annual minimum sea-ice extent in September 2020 was the second lowest on record, and record low sea-ice extent was observed in the months of July and October. The sea-ice extents in April, August, November, and December were among the five lowest in the 42-year satellite data record. For more details on the data sets used, see Sea-ice data.

In the Arctic, the maximum sea-ice extent for the year was reached on 5 March 2020. At just above 15 million km², this was the 10th or 11th (depending on the data set used) lowest maximum extent on record.[28] Sea-ice retreat in late March was mostly in the Bering Sea. In April, the rate of decline was similar to that of recent years, and the mean sea-ice extent for April was between the second and fourth lowest on record, effectively tied with 2016, 2017, and 2018 (Figure 10).

Record high temperatures north of the Arctic Circle in Siberia (see The Arctic in 2020) triggered an acceleration of sea-ice melt in the East Siberian and Laptev Seas, which continued well into July. The sea-ice extent for July was the lowest on record (7.28 million km²).[29] The sea-ice retreat in the Laptev Sea was the earliest observed in the satellite era. Towards the end of July, a cyclone entered the Beaufort Sea and spread

[27] FAIR principles: https://www.go-fair.org/fair-principles/

[28] http://nsidc.org/arcticseaicenews/2020/03/

[29] https://cryo.met.no/en/arctic-seaice-summer-2020, https://nsidc.org/arcticseaicenews/2020/08/steep-decline-sputters-out/

the sea ice out, temporarily slowing the decrease of the ice extent. In mid-August, the area affected by the cyclone melted rapidly, which, combined with the sustained melt in the East Siberian and Laptev Seas, made the August extent the 2nd or 3rd lowest on record.

The 2020 Arctic sea-ice extent minimum was observed on 15 September to be 3.74 million km^2, marking only the second time on record that the Arctic sea-ice extent shrank to less than 4 million km^2. Only 2012 had a lower minimum extent at 3.39 million km^2. Vast areas of open ocean were observed in the Chukchi, East Siberian, Laptev, and Beaufort Seas, notwithstanding a tongue of multi-year ice that survived the 2020 melt season in the Beaufort Sea (Figure 13).[30]

Refreeze was slow in late September and October in the Laptev and East Siberian Seas, probably due to the heat accumulated in the upper ocean since the early retreat in late June. The Arctic sea-ice extent was the lowest on record for October and November. December sea-ice growth was faster than average, but the extent remained the second or third lowest on record for the month.

Interannual variability in the annual mean extent of Antarctic sea ice has increased since 1979. For the first 20 years of measurements from 1979 to 1999, there was no significant trend; however, around 2002, the total extent began to increase, reaching a maximum of 12.8 million km^2 in 2014. This was followed by a remarkable decrease over the next three years to a record minimum of 10.7 million km^2 in 2017. The decrease occurred in all sectors but was greatest in the Weddell Sea sector.

In 2020, the Antarctic sea ice extent increased to 11.5 million km^2, only 0.14 million km^2 below the long-term mean. Indeed, extents were close to the long-term mean in all sectors. The Bellingshausen Sea sector had its lowest extent on record in July 2020, but the extent was closer to the mean later in the year.

The Antarctic sea-ice extent in January 2020 showed only a modest increase from the very low values of the previous years, but February 2020 saw a return to less extreme conditions. During the autumn and winter of 2020, the Antarctic sea-ice extent was mostly close to the long-term mean but with positive ice extent anomalies near the maximum in September and October.

The minimum Antarctic sea ice extent in 2020 was around 2.7 million km^2. This occurred between 19 February and 2 March (depending on the data set) and was the seventeenth lowest minimum in the record. It reflected the gradual increase from the record minimum extent of 2.08 million km^2 on 1 March 2017. The maximum extent of the Antarctic sea ice in 2020 was around 19 million km^2 and was observed between 26 and 28 September. This was the thirteenth largest extent in the 42-year record.

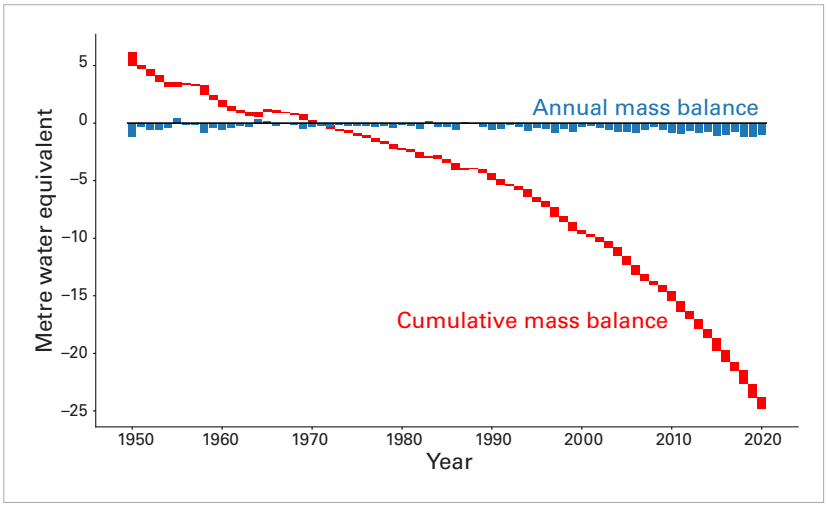

Figure 11. Annual (blue) and cumulative (red) mass balance of reference glaciers with more than 30 years of ongoing glaciological measurements. Global mass balance is based on an average for 19 regions to minimize bias towards well-sampled regions. Annual mass changes are expressed in metre water equivalent (m w.e.), which corresponds to tons per square metre (1 000 kg m^{-2}). *Source:* World Glacier Monitoring Service, 2021, updated

GLACIERS

Glaciers are formed from snow that has compacted to form ice, which can deform and flow downhill to lower, warmer altitudes, where it melts, or if the glacier terminates in the ocean, breaks up, forming icebergs. Glaciers are sensitive to changes in temperature, precipitation and incoming solar radiation, as well as other factors, such as changes in basal lubrication or the loss of buttressing ice shelves.

According to the World Glacier Monitoring Service (Figure 11), in the hydrological year 2018/2019, the roughly 40 glaciers with

[30] https://cryo.met.no/en/arctic-seaice-september-2020

long-term observations experienced an ice loss of 1.18 metre water equivalent (m w.e.), close to the record loss set in 2017/2018. Despite the global pandemic, observations for 2019/2020 were able to be collected for the majority of the important glacier sites worldwide, although some data gaps will be inevitable. Preliminary results for 2020, based on a subset of evaluated glaciers, indicate that glaciers continued to lose mass in the hydrological year 2019/2020. However, mass balance was slightly less negative, with an estimated ice loss of 0.98 m w.e.

The lower rates of glacier mass change are attributed to more moderate climate forcing in some regions, for example in Scandinavia, High Mountain Asia and, to a lesser extent, North America. Lower rates are in some cases explained by high winter precipitation. Most other regions, such as the European Alps or New Zealand, showed strong glacier mass loss, albeit less than in the two preceding years. In contrast, there are indications that glaciers in the Arctic, which account for a large area, were subject to substantially increased melting, but data are still too scarce to establish the overall signal. Although the hydrological year 2019/2020 was characterized by somewhat less negative glacier mass balances in many parts of the Earth, there is a clear trend towards accelerating glacier mass loss in the long term, which is also confirmed by large-scale remote sensing studies. Eight out of the ten most negative mass balance years have been recorded since 2010.

ICE SHEETS

Despite the exceptional warmth in large parts of the Arctic, in particular the very unusual temperatures that were observed in eastern Siberia, temperatures over Greenland in 2020 were close to the long-term mean (Figure 2). The Greenland ice sheet ended the September 2019 to August 2020 season with an overall loss of 152 Gt of ice. This loss was a result of surface melting, the discharge of icebergs and the melting of glacier tongues by warm ocean water (Figure 12) and although significant, was less than the loss of ice in the previous year (329 Gt).

Changes in the mass of the Greenland ice sheet reflect the combined effects of the surface mass balance (SMB) – defined as the difference between snowfall and run-off from the ice sheet, which is always positive at the end of the year – and mass losses at the periphery from the calving of icebergs and the melting of glacier tongues that meet the ocean. The 2019/2020 Greenland SMB was +349 Gt of ice, which is close to the 40-year average of +341 Gt. However, ice loss due to iceberg calving was at the high end of the 40-year satellite record. The Greenland SMB record is now four decades long and, although it varies from one year to another, there has been an overall decline in the average SMB over time (Figure 12). In the 1980s and 1990s, the average SMB gain was about +416 Gt/year. It fell to +270 Gt/year in the 2000s and +260 Gt/year in the 2010s.

The GRACE satellites and the follow-on mission GRACE-FO measure the tiny change of the gravitational force due to changes in the amount of ice. This provides an independent measure of the total mass balance. Based on this data, it can be seen that the Greenland ice sheet lost about 4 200 Gt from April 2002 to August 2019, which contributed to a sea-level rise of slightly more than 1 cm. This is in good agreement with the mass balance from SMB and discharge, which was 4 261 Gt during the same period.

The 2019/2020 melt season on the Greenland ice sheet started on 22 June, 10 days later than the 1981–2020 average. As in previous seasons, there were losses along the Greenlandic west coast and gains in the east. In mid-August, unusually large storms

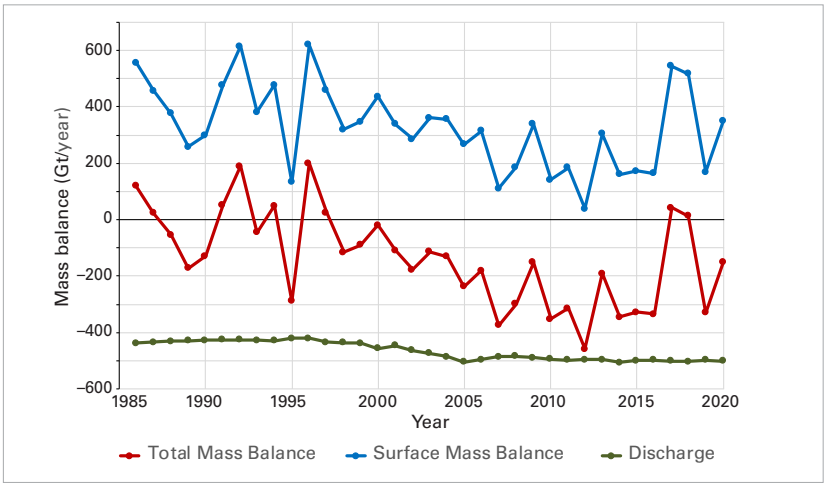

Figure 12. Components of the total mass balance of the Greenland ice sheet for the period 1986–2020. Blue: surface mass balance (http://polarportal.dk/en/greenland/surface-conditions/), green: discharge, red: total mass balance (the sum of the surface mass balance and discharge). *Source:* Mankoff, K.D. et al., 2020: Greenland Ice Sheet solid ice discharge from 1986 through March 2020. *Earth System Science Data*, 12(2): 1367–1383, https://doi.org/10.5194/essd-12-1367-2020.

The Arctic in 2020

The Arctic has been undergoing drastic changes as the global temperature has increased. Since the mid-1980s, Arctic surface air temperatures have warmed at least twice as fast as the global average, while sea ice, the Greenland ice sheet and glaciers have declined over the same period and permafrost temperatures have increased. This has potentially large implications not only for Arctic ecosystems, but also for the global climate through various feedbacks.[a]

In 2020, the Arctic stood out as the region with the largest temperature deviations from the long-term average. Contrasting conditions of ice, heat and wildfires were seen in the eastern and western Arctic (Figure 13). A strongly positive phase of the Arctic Oscillation during the 2019/2020 winter set the scene early in the year, with higher-than-average temperatures across Europe and Asia and well-below-average temperatures in Alaska, a pattern which persisted throughout much of the year.

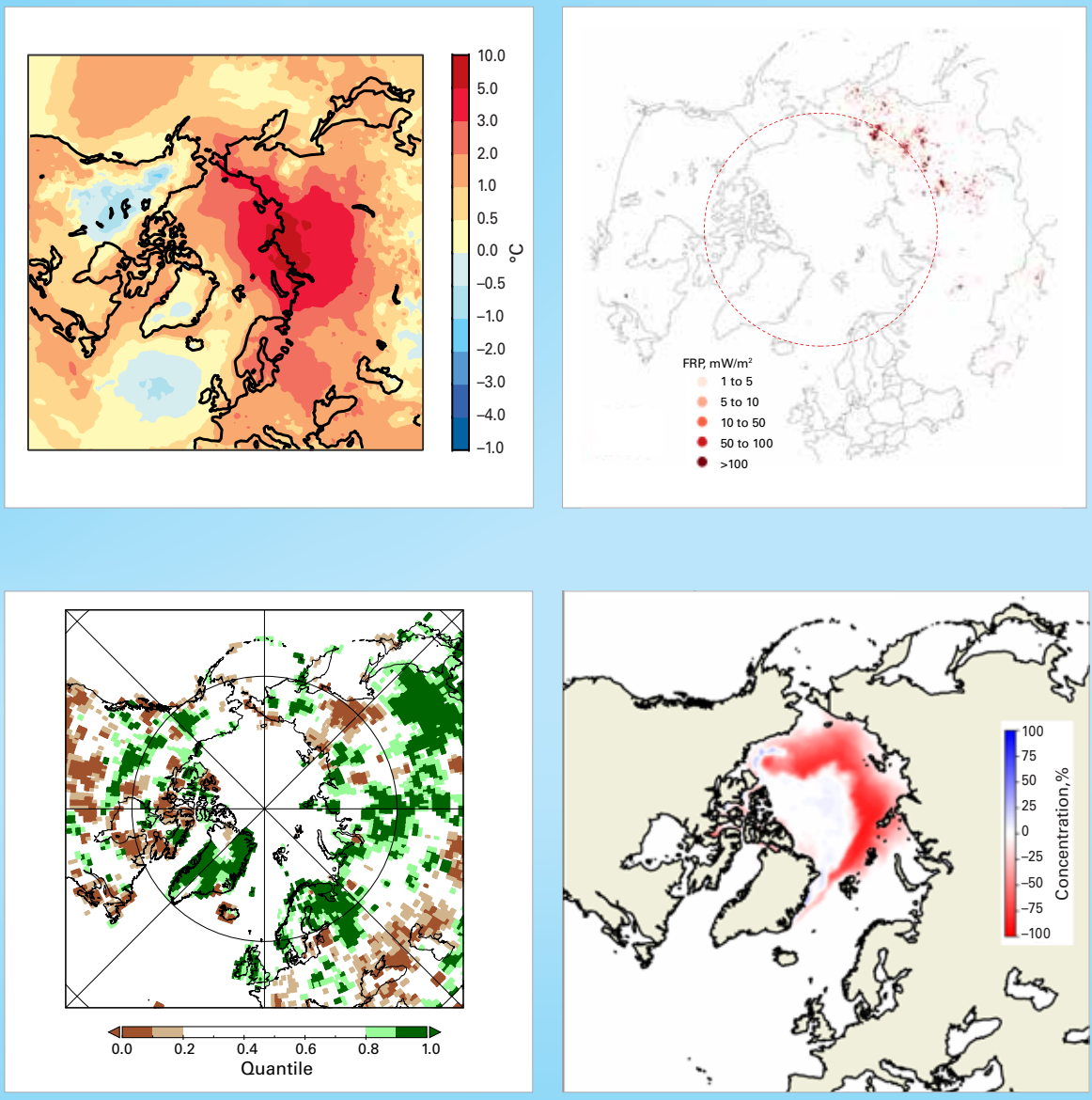

Figure 13. Top left: Temperature anomalies for the Arctic relative to the 1981–2010 long-term average from the ERA5 reanalysis for 2020. *Source:* Copernicus Climate Change Service, ECMWF

Top right: Fire Radiative Power, a measure of heat output from wildfires, in the Arctic Circle between June and August 2020. *Source:* Copernicus Atmosphere Monitoring Service, ECMWF

Bottom left: Total precipitation in 2020, expressed as a percentile of the 1951–2010 reference period, for areas that would have been in the driest 20% (brown) and wettest 20% (green) of years during the reference period, with darker shades of brown and green indicating the driest and wettest 10%, respectively. *Source:* Global Precipitation Climatology Centre (GPCC)

Bottom right: Sea-ice concentration anomaly for September 2020. *Source:* EUMETSAT OSI SAF v2p1 data, with research and development input from the European Space Agency Climate Change Initiative (ESA CCI)

[a] Intergovernmental Panel on Climate Change, 2019: *IPCC Special Report on the Ocean and Cryosphere in a Changing Climate*, https://www.ipcc.ch/srocc/.

In a large region of the Siberian Arctic, temperature anomalies for 2020 were more than 3 °C, and in its central coastal parts, more than 5 °C above average (Figure 13). A preliminary record temperature of 38 °C was set for north of the Arctic Circle, on 20 June in Verkhoyansk,[b] during a prolonged heatwave. Heatwaves and heat records were also observed in other parts of the Arctic (see High-impact events in 2020), and extreme heat was not confined to the land. A marine heatwave affected large areas of the Arctic Ocean north of Eurasia (Figure 8). Sea ice in the Laptev Sea, offshore from the area of highest temperature anomalies on land, was unusually low through the summer and autumn. Indeed, the sea-ice extent was particularly low along the Siberian coastline, with the Northern Sea Route ice-free or close to ice-free from July to October. The high spring temperatures also had a significant effect on other parts of the cryosphere. June snow cover was the lowest for the Eurasian Arctic in the 54-year satellite record despite the region having a larger-than-average extent as late as April.[c]

Although the Arctic was predominantly warmer than average for this period, some regions, including parts of Alaska and Greenland, saw close to average or below-average temperatures. As a result, the 2019/2020 surface mass balance for Greenland was close to the 40-year average. Nevertheless, the decline of the Greenland ice sheet continued during the 2019/2020 season, but the loss was below the typical amounts seen during the last decade (see Cryosphere). Sea-ice conditions along the Canadian archipelago were close to average at the September minimum, and the western passage remained closed.[d]

The wildfire season in the Arctic during 2020 was particularly active, but with large regional differences. The region north of the Arctic circle saw the most active wildfire season in an 18-year data record, as estimated in terms of fire radiative power and CO_2 emissions released from fires. The main activity was concentrated in the eastern Siberian Arctic, which was also drier than average. Regional reports[e] for eastern Siberia indicate that the forest fire season started earlier than average, and for some regions ended later, resulting in long-term damage to local ecosystems. Alaska, as well as the Yukon and the Northwest Territories, reported fire activity that was well below average.

[b] https://public.wmo.int/en/media/news/reported-new-record-temperature-of-38%C2%B0c-north-of-arctic-circle

[c] Mudryk, L.E. et al., 2020: *Arctic Report Card 2020: Terrestrial Snow Cover. United States. National Oceanic and Atmospheric Administration.* Office of Oceanic and Atmospheric Research University of Toronto. Department of Physics Ilmatieteen laitos (Finland) / Finnish Meteorological Institute, https://doi.org/10.25923/P6CA-V923.

[d] Arctic Climate Forum, https://arctic-rcc.org/sites/arctic-rcc.org/files/presentations/acf-fall-2020/2%20-%20Day%202%20-%20ACF-6_Arctic_summary_MJJAS_2020_v2.pdf

[e] Arctic Climate Forum, https://arctic-rcc.org/sites/arctic-rcc.org/files/presentations/acf-fall-2020/3%20-%20Day%201-%20ACF%20October%202020%20Regional%20Overview%20Summary%20with%20extremes%20-281020.pdf

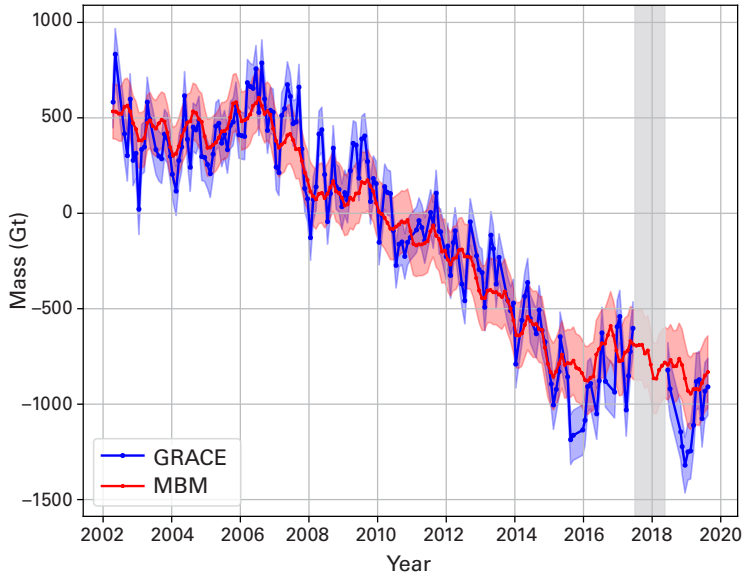

Figure 14. Comparison of Antarctic ice sheet mass changes from GRACE/GRACE-FO satellite gravimetry (blue) and the mass budget method (MBM) (red). This comparison highlights the large interannual variability in mass change, the relatively large uncertainties in these two methods, and their occasional disagreement. *Source:* Velicogna et al., 2020 (see reference details in Antarctic ice sheet data)

brought four times the normal monthly precipitation to western Greenland, most of which fell as snow that temporarily stopped the net loss of ice and was decisive in reducing the amount of melt; this was quite different from the situation in the previous season (2018/2019), in which there were extended high pressure periods and large amounts of sunshine, which significantly increased the summer melt.

There is no routine reporting of the annual mass balance for the Antarctic ice sheet, and reported mass changes typically have a latency of several years. This is because multiple data sets must be combined to reduce uncertainty and bias in mass-change estimates on the continental scale.

Antarctica has exhibited a strong mass loss trend since the late 1990s. This trend accelerated around 2005, and currently, Antarctica loses approximately 175 to 225 Gt per year. Nearly 90% of the acceleration of this trend is due to the increasing flow rates of major glaciers in West Antarctica and the Antarctic Peninsula.[17] This is in contrast to the Greenland ice sheet, where losses from surface melting are of comparable magnitude to those from glacier dynamics. The main driver of faster glacier flow in Antarctica has been enhanced sub-sea melting of fringing ice shelves, with a secondary driver being abrupt ice-shelf collapse due to localized surface melting on the Antarctic Peninsula.[39] This glacier-dynamic response to climate and ocean forcing is strongly controlled by thresholds (ice shelf collapse) and strongly modulated by positive feedbacks in flow. As a result, Antarctica's interannual dynamic losses are largely uncoupled from fluctuations in weather on annual timescales.

Superimposed on this sustained mass loss trend is a large interannual variability in snowfall that fluctuates by several hundred gigatons (Figure 14) around an average of approximately 2 300 Gt to 2 500 Gt per year[31] and has no clear trend over recent decades.[32] These large fluctuations are dominated spatially and temporally by occasional extreme snowfall events.[33] Instrumental observations of snowfall on the continent are extremely scarce, however, and ice-sheet mass changes are instead calculated retrospectively from satellite-observed changes in flow rate (the mass budget method), the gravity field or surface height, combined with modelled surface mass balance, near-surface snow density and isostatic rebound, respectively. Each of these three sets of observations and associated model inputs contains significant uncertainties and potential biases, and the results reported by these techniques do not always agree within their uncertainties.[34] Consensus on Antarctic mass changes therefore emerges only from a detailed inter-comparison of this suite of methods, with careful consideration of their respective strengths and weaknesses.[39,43] No such consensus value is available yet for the 2019/2020 period.

[31] Mottram, R. et al., 2020: What Is the Surface Mass Balance of Antarctica? An Intercomparison of Regional Climate Model Estimates. *The Cryosphere Discussions*, 1–42, https://doi.org/10.5194/tc-2019-333.

[32] King, M.A. and C.S. Watson, 2020: Antarctic Surface Mass Balance: Natural Variability, Noise, and Detecting New Trends. *Geophysical Research Letters*, 47(12): e2020GL087493, https://doi.org/10.1029/2020GL087493.

[33] Turner, J. et al., 2019: The Dominant Role of Extreme Precipitation Events in Antarctic Snowfall Variability. *Geophysical Research Letters*, 46(6): 3502–3511, https://doi.org/10.1029/2018GL081517.

[34] Shepherd, A. et al., 2018: Mass Balance of the Antarctic Ice Sheet from 1992 to 2017. *Nature*, 558(7709): 219–222, https://doi.org/10.1038/s41586-018-0179-y.

PRECIPITATION

Annual precipitation totals in monsoon-influenced regions in North America, Africa, South-West Asia and South-East Asia were unusually high in 2020 (Figure 15, top), as were extreme daily totals (expressed as the 95th percentile of daily totals) (Figure 15, bottom). The African Monsoon extended farther north into the Sahel region than usual. Monsoon seasonal totals in India were 109% of the long-term mean, the third highest seasonal total after 1994 and 2019. East Asia experienced abnormally high annual and extreme daily rainfall totals.

In other regions, the extreme daily totals (95th percentile of daily precipitation amounts) were lower than the long-term mean (Figure 15, bottom), for example, the Maritime Continent (incorporating Indonesia, Papua New Guinea and the Philippines, as well as other islands in the region), Central and North-West Africa, large areas of the Americas and Central and West Europe.

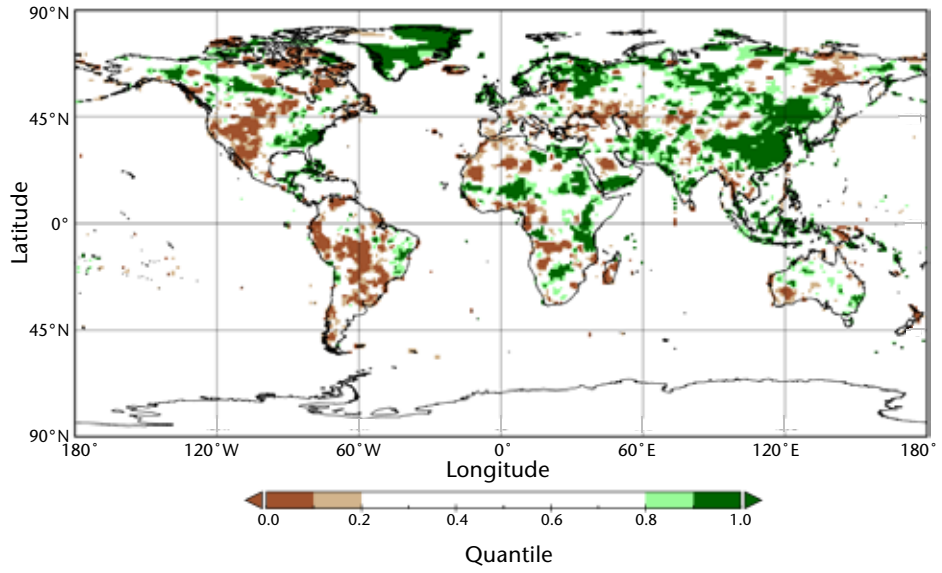

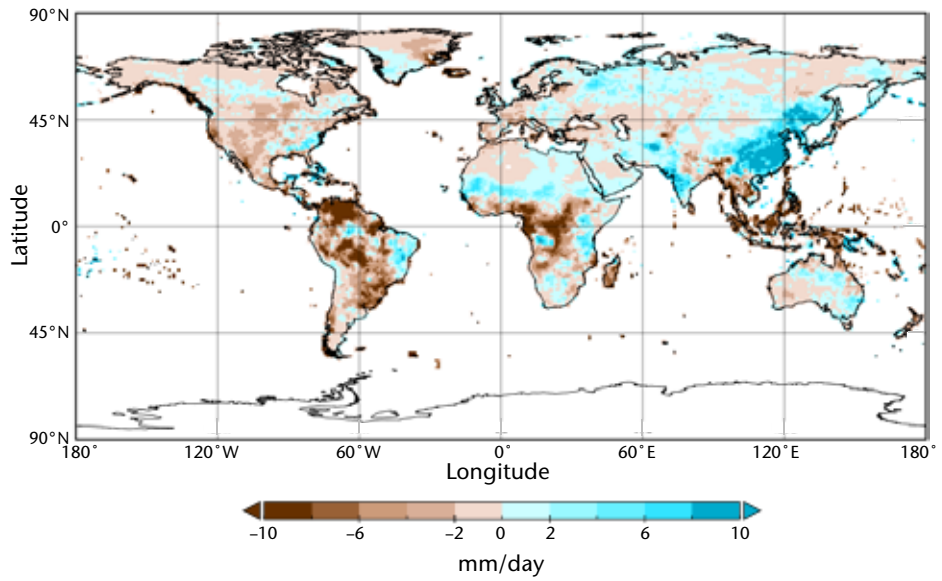

Figure 15. Top: Total precipitation in 2020, expressed as a percentile of the 1951–2010 reference period. The shaded areas are those with precipitation totals in the driest 20% (brown) and wettest 20% (green) of years during the reference period, with darker shades of brown and green indicating the driest and wettest 10%, respectively.
Note: A longer reference period is used here because precipitation is more variable, and a longer period allows a more reliable long-term average to be calculated.
Bottom: Difference between the observed 95th percentile of daily precipitation total in 2020 and the long-term mean based on the 1982–2016 (full year) period. Blue indicates more extreme daily precipitation events than the long-term mean, and brown indicates fewer extreme daily precipitation events than the long-term mean.
Note: The period used here is the full length of the global daily precipitation data set.
Source: GPCC, Deutscher Wetterdienst, Germany

DRIVERS OF SHORT-TERM CLIMATE VARIABILITY

There are many different natural phenomena, often referred to as climate patterns or climate modes, that affect weather at timescales ranging from days to several months. Surface temperatures change relatively slowly over the ocean, so recurring patterns in sea-surface temperature can be used to understand, and in some cases, predict the more rapidly changing patterns of weather over land on seasonal timescales. Similarly, albeit at a faster rate, known pressure changes in the atmosphere can help explain certain regional weather patterns.

In 2020, the El Niño–Southern Oscillation (ENSO) and the Arctic Oscillation (AO) each contributed to weather and climate events in different parts of the world. The Indian Ocean Dipole, which played a key role in the events of 2019, was near-neutral for much of 2020.

EL NIÑO–SOUTHERN OSCILLATION

ENSO is one of the most important drivers of year-to-year variability in weather patterns around the world. It is linked to hazards such as heavy rains, floods, and drought. El Niño, characterized by higher-than-average sea-surface temperatures in the eastern Pacific and a weakening of the trade winds, typically has a warming influence on global temperatures. La Niña, which is characterized by below-average sea-surface temperatures in the central and eastern Pacific and a strengthening of the trade winds, has the opposite effect.

Sea-surface temperatures at the end of 2019 were close to or exceeded El Niño thresholds in the Niño 3.4 region.[4] These temperatures persisted into the early months of 2020, but the event did not strengthen, and sea-surface temperature anomalies in the eastern Pacific fell in March. After a six-month period of neutral conditions – that is, sea-surface temperatures within 0.5 °C of normal – the cool-phase, La Niña, developed in August and strengthened through the northern hemisphere autumn to moderate strength (1.0–1.5 °C below normal). The atmosphere also responded with stronger-than-average trade winds, indicating a coupling with the sea-surface temperatures. La Niña conditions are associated with above-average hurricane activity in the North Atlantic, which experienced a record number of named tropical storms during its 2020 hurricane season, and also with above-average rainfall in Australia, which ended the year with its fourth wettest December on record.

ARCTIC OSCILLATION

AO is a large-scale atmospheric pattern that influences weather throughout the northern hemisphere. The positive phase is characterized by lower-than-average air pressure over the Arctic and higher-than-average pressure over the northern Pacific and Atlantic Oceans. The jet stream is parallel to the lines of latitude and farther north than average, locking up cold Arctic air, and storms can be shifted northward of their usual paths. The mid-latitudes of North America, Europe, Siberia, and East Asia generally see fewer cold air outbreaks than usual during the positive phase of AO. A negative AO has the opposite effect and is associated with a more meandering jet stream and cold air spilling south into the mid-latitudes.

AO was strongly positive during the northern hemisphere 2019/2020 winter and in February was the strongest it had been since January 1993. This contributed to the warmest winter on record for Asia and Europe and the sixth warmest winter on record for the contiguous United States; at the same time, Alaska experienced its coldest winter in more than two decades. By containing cold air in the polar region through the entire winter, the positive AO also contributed to a relatively rare and record-large Arctic ozone hole in March (see Stratospheric ozone and ozone-depleting gases). Additionally, the positive winter phase of AO has been linked to low sea-ice extent the following summer[35] (see Sea ice). AO was strongly positive in November but rapidly declined to large negative values in December and in early 2021.

[35] Rigor, I.G. et al., 2002: Response of Sea Ice to the Arctic Oscillation. *Journal of Climate*, 15(18): 2648–2663, https://doi.org/10.1175/1520-0442(2002)015%3c2648:ROSITT%3e2.0.CO;2.

High-impact events in 2020

Although understanding broad-scale changes in the climate is important, the most acute impacts of weather and climate are often felt during extreme meteorological events such as heavy rain and snow, droughts, heatwaves, cold waves, and storms, including tropical storms. These can lead to or exacerbate other high-impact events such as flooding, landslides, wildfires, and avalanches. The risks and impacts associated with these events are described in Risks and impacts.

A YEAR OF WIDESPREAD FLOODING, ESPECIALLY IN AFRICA AND ASIA

Very extensive flooding occurred over large parts of Africa in 2020. Rainfall was well above average in most of the Greater Horn of Africa during the March–May "long rains" season, following a similarly wet season in October–December 2019. This was followed by above-average rainfall across the vast majority of the Sahel region, from Senegal to Sudan, during the summer monsoon (Figure 15).

Flooding was extensive across many parts of the region, although Sudan and Kenya were the worst affected, with 285 deaths reported in Kenya,[36] and 155 deaths and over 800 000 people affected in Sudan,[37] along with further indirect impacts from disease. Countries reporting loss of life or significant displacement of populations included Sudan, South Sudan, Ethiopia, Somalia, Kenya, Uganda, Chad, Nigeria (which also experienced drought in the southern part of the country), Niger, Benin, Togo, Senegal, Côte d'Ivoire, Cameroon and Burkina Faso. Many lakes and rivers reached record high levels, including Lake Victoria in May and the Niger River at Niamey and the Blue Nile at Khartoum in September.

India had one of its two wettest monsoon seasons since 1994, with nationally-averaged rainfall for June to September 9% above the long-term average. Heavy rain, flooding and landslides also affected the surrounding countries. August was the wettest month on record for Pakistan, and 231 mm of rain fell on 28 August at Karachi-Faisal, the highest daily total on record in the Karachi area. More than 2 000 deaths were reported during the monsoon season in India, Pakistan, Nepal, Bangladesh, Afghanistan and Myanmar,[36] including 145 deaths associated with flash flooding in Afghanistan in late August and 166 deaths associated with a landslide at a mine in Myanmar in early July following heavy rain.

Persistent high rainfall in the Yangtze River catchment in China in the monsoon season also caused severe flooding. The June–August period was particularly wet, and floods affected the Yangtze and its tributaries. In mid-August, the Three Gorges Dam saw the largest flood peak since its construction, reaching 75 000 m^3s^{-1}. The summer monsoon season over the Korean Peninsula was also very wet, with the Republic of Korea experiencing its third-wettest summer, and parts of western Japan were affected by significant flooding in July.

Parts of South-East Asia experienced severe flooding in October and November. The

Flooding in the coastal city of Pointe Noire, Congo on 6 February 2020

Credit: Leo Toreton, International Organization for Migration/ Central African Republic

[36] EM-DAT, https://www.emdat.be/

[37] Reliefweb, Situation Report, Sudan, 13 November 2020, https://reliefweb.int/sites/reliefweb.int/files/resources/Situation%20Report%20-%20Sudan%20-%2013%20Nov%202020.pdf

worst affected area was Central Viet Nam, where heavy rains typical of the arrival of the north-east monsoon were exacerbated by a succession of tropical cyclones and depressions, with eight making landfall in less than five weeks. Hué received over 1 800 mm of rain in the week of 7 to 13 October, and a total of 2 615 mm for the month of October. The flooding also extended further west into Cambodia.

Other regions which experienced a significant loss of life associated with floods (mostly flash floods resulting from extreme local rainfall) included Indonesia in January, Brazil in January and March, the Democratic Republic of the Congo and Rwanda in April and May, and Yemen in July. Jakarta had its wettest day since 1996, with 377 mm of rainfall recorded at Halim Airport on 1 January, and Belo Horizonte, Brazil experienced its wettest day on record, with 172 mm of rainfall recorded on 24 January. Khombole, Senegal also experienced its wettest day on record, with 226 mm of rainfall recorded on 5 September.

HEATWAVES, DROUGHT AND WILDFIRE

Severe drought affected many parts of the interior of South America in 2020, with the worst-affected areas being northern Argentina, Uruguay, Paraguay and the western border areas of Brazil. Most of the provinces of northern Argentina had one of their five driest years on record, with Buenos Aires experiencing its second driest year. Rainfall for the period was also far below average in Paraguay and Uruguay. Estimated agricultural losses were near US$ 3 billion in Brazil, with additional losses in Argentina, Uruguay and Paraguay. River levels were so low that river transport in Paraguay was disrupted. Peru also experienced drought conditions between January and March, mainly in the north of the country.[38] As the drought continued, a major heatwave stretched across the region in late September and early October, extending east and north to cover much of the interior of Brazil. The temperature reached 44.6 °C on 5 October at Nova Maringá and Água Clara, and individual locations which had their hottest day on record included Cuiaba, Curitiba, Belo Horizonte and Asuncion. There was significant wildfire activity across Argentina, Brazil and Paraguay from mid-year onwards, with some of the most serious wildfires occurring in the Pantanal wetlands in western Brazil.

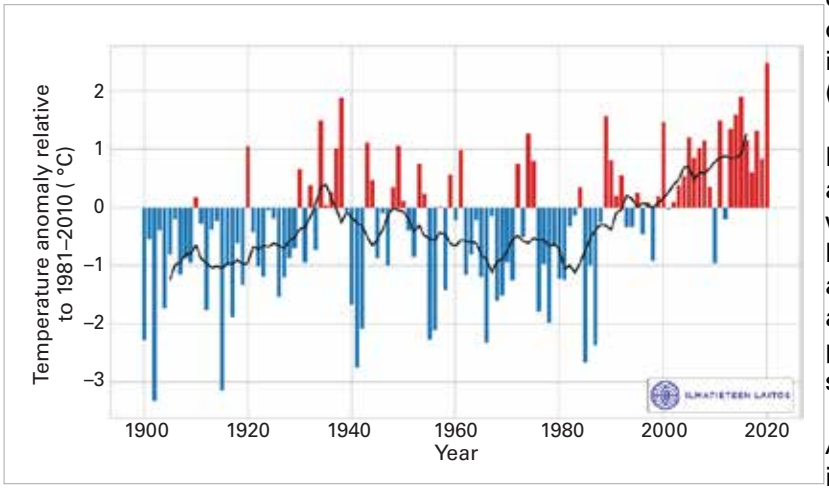

Figure 16. Annual average temperature in Finland relative to the 1981–2010 average. The black curve shows the 10-year moving average of the temperature anomaly.
Source: Finnish Meteorological Institute

2020 was an exceptionally warm year for most of Russia, especially Siberia. Temperatures averaged over Russia for 2020 were 3.2 °C above average, 1.0 °C above the previous record set in 2007. In parts of northern Siberia, mean temperatures for the year were 6 °C or more above average. The heat culminated in late June, when temperatures reached 38.0 °C at Verkhoyansk on 20 June, provisionally the highest known temperature anywhere north of the Arctic Circle. Abnormal warmth also extended to other parts of the high Arctic outside Russia, with temperatures reaching records on 25 July of 21.9 °C at Eureka (Canada), and 21.7 °C at Svalbard Airport.

Finland set new national highest temperature records in 2020, which was also the warmest year for the country overall. The highest annual mean temperature among all stations in Finland was 9.2 °C, recorded at Utö, Pargas. This was 0.8 °C above the previous national record set at the same station in 2015 (Figure 16).

A number of exceptionally large wildfires, including the largest fires ever recorded

[38] https://cdn.www.gob.pe/uploads/document/file/1325635/INFORME-LLUVIAS-2019-2020%20FINAL-29-09-2020v2.pdf

in the states of California and Colorado, occurred in the western United States in late summer and autumn, contributing to the largest area burned nationally in the last 20 years. Widespread drought conditions through the western half of the United States, particularly the interior south-west, contributed to the fires, as did a very weak summer monsoon. The three-month period from July to September was the hottest and driest on record for the south-west United States, and 2020 was the driest year on record for Nevada and Utah. Abnormal lightning activity in coastal California in mid-August also ignited many fires. The most destructive fires were in California and western Oregon, with over 8 500 structures destroyed in California and over 2 000 destroyed in Oregon; 46 deaths and US$ 16.5 billion in losses were attributed to the fires across multiple states.[39] There were also a number of episodes of extreme heat. Death Valley reached 54.4 °C on 16 August, the highest known temperature in the world in at least the last 80 years, while 49.4 °C was reached on 6 September at Woodland Hills, which was a record for greater Los Angeles. The highest temperature ever recorded was 56.7 °C and was reached at Furnace Creek, California on 10 July 1911. A temperature of 55.0 °C was recorded in Kebili, Tunisia on 7 July 1931;[40] this was a record for the eastern hemisphere.

Major wildfires in eastern Australia which had burned throughout the later part of 2019 continued into early 2020 before finally being controlled after heavy rain in early February. Drought conditions, which had prevailed since early 2017, eased from January 2020 onwards, but there were a number of episodes of extreme heat in early 2020. Penrith, in western Sydney, reached 48.9 °C, the highest temperature observed in an Australian metropolitan area, on 4 January, while Canberra, which set monthly records in all three summer months, reached a new high of 44.0 °C on the same day. Severe smoke pollution also affected many parts of south-eastern Australia in the early part of 2020. A number of stations in New Zealand reported their longest dry spell on record between late December 2019 and late February 2020.

A major heatwave affected the Caribbean region and Mexico in April. Temperatures reached 39.7 °C at Veguitas on 12 April, a national record for Cuba, and Havana also had its hottest day on 12 April, with temperatures reaching 38.5 °C. In eastern Mexico, temperatures exceeded 45 °C at a number of locations, reaching as high as 48.8 °C at Gallinas on 12 April, while very high readings in Central America included 41.2 °C at San Agustin Acasaguastlán (Guatemala). Further extreme heat in September saw national or territorial records set for Dominica, Grenada and Puerto Rico.

Dry conditions affected parts of North-Central Europe during the spring and summer of 2020 although generally not to the same extent as in 2018 or 2019. April was especially dry, with Romania and Belarus having their driest April on record, and Germany, the Czech Republic

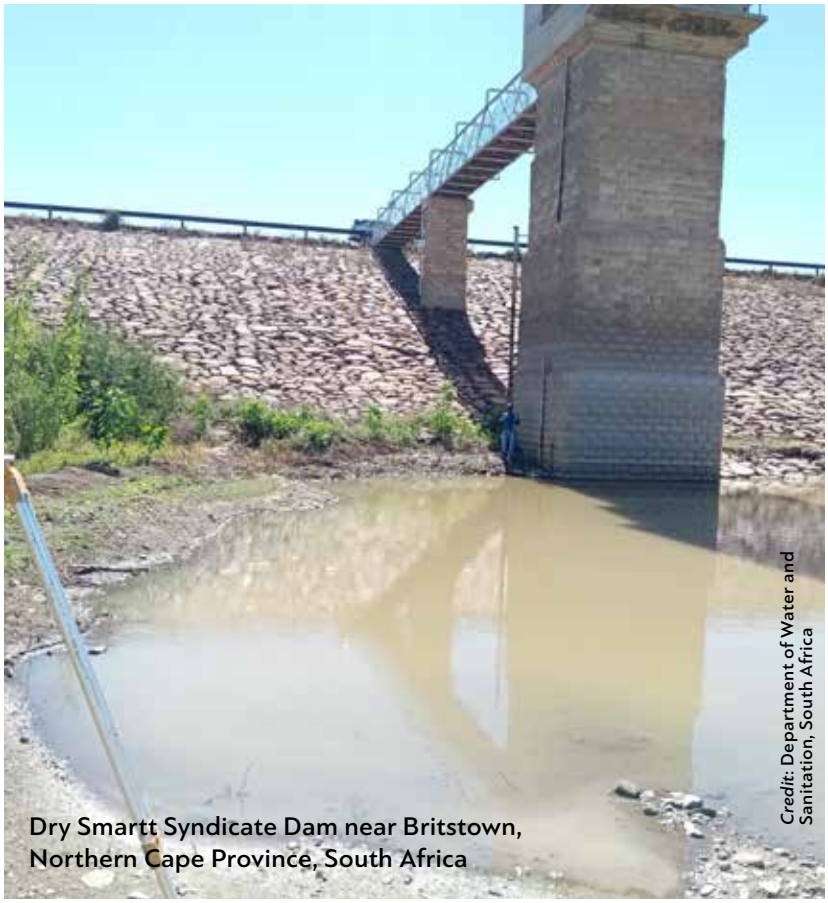

Dry Smartt Syndicate Dam near Britstown, Northern Cape Province, South Africa

Credit: Department of Water and Sanitation, South Africa

[39] NOAA National Centers for Environmental Information (NCEI) U.S. Billion-Dollar Weather and Climate Disasters (2021), https://www.ncdc.noaa.gov/billions/.

[40] https://wmo.asu.edu/content/world-meteorological-organization-global-weather-climate-extremes-archive

and Slovak Republic their second driest, while Geneva (Switzerland) had a record 43-day dry spell from 13 March to 24 April. There was also a significant heatwave in western Europe in August; while it was generally not as intense as those of 2019 (except locally on the northern coast of France), many locations, particularly in northern France, reached temperatures which ranked second behind the 2019 heatwaves, and De Bilt (Netherlands) had a record eight consecutive days above 30 °C. In early September, the focus of extreme heat shifted to the eastern Mediterranean, with all-time records at locations including Jerusalem (42.7 °C) and Eilat (48.9 °C) on 4 September following a late July heatwave in the Middle East in which temperatures at Kuwait Airport reached 52.1 °C and temperatures at Baghdad reached 51.8 °C.

The summer was very hot in parts of East Asia. Hamamatsu (41.1 °C) equalled Japan's national record on 17 August, and Taipei had its hottest day on record on 24 July, with temperatures reaching 39.7 °C. Hong Kong had a record run of 13 consecutive hot nights, with a daily minimum temperature of 28 °C or above, from 19 June to 1 July, followed by 11 consecutive hot nights from 5 to 15 July.

Long-term drought continued to persist in parts of southern Africa, particularly the Northern and Eastern Cape Provinces of South Africa, although heavy winter rains saw water storages reach full capacity in Cape Town, continuing the recovery from the extreme drought situation which peaked in 2018. Rainfall during the 2019/2020 summer rainy season in the interior of southern Africa was locally heavy, and many areas had above-average rainfall in November and December; however long-term drought still persisted in some areas.

EXTREME COLD AND SNOW

North America's most significant snowstorm of the 2019/2020 winter occurred on 17–18 January in Newfoundland. St. John's received 76.2 cm of snow, including a record daily snowfall, and wind gusts reached 126 km/h. Later in the year, there were two extreme early-season cold episodes in autumn. In the second week of September, widespread snowfalls occurred in lowland Colorado, including Denver, where a September record high temperature of 38.3 °C had been set only three days earlier on 5 September.

Later, in October, a major cold outbreak brought exceptionally low temperatures and winter precipitation across a broad region of the Rocky Mountains and central states. A damaging ice storm in Oklahoma City saw power outages which lasted for days across more than half the city, while further north, Potomac, Montana reached –33.9 °C on 25 October, the earliest autumn date on which temperatures had fallen below –30 °C at a climate station anywhere in the United States (excluding Alaska).

The extremely wet and warm winter in northern Europe resulted in exceptionally low snow cover in many places – Helsinki experienced a record low number of snow-covered days, breaking the previous record by a wide margin – but in far northern Europe, where temperatures were above average but still cold enough for snow, the snowpack was exceptionally heavy. At Sodankylä (Finland), the snowpack reached a record depth of 127 cm in mid-April. A cold May led to a delayed melt with some cover persisting into June, while flooding occurred in late May and early June with the spring melt. Rain-on-snow events prevented some reindeer herds from reaching feed.

The 2020 winter was cold in southern South America. Tierra del Fuego had its most significant cold spell since 1995 in late June and early July, with Rio Grande recording a maximum of –8.8 °C and a minimum of –16.5 °C on 1 July. Paraguay saw record minimum temperatures for August in a number of places. Snow cover in Patagonia was the second-most extensive since 2000 and sea ice formed along parts of the Tierra del Fuego coast. Some stock losses were reported. In August, a cold wave in the north of Peru's Amazonia saw temperatures at Caballococha reach 12.8 °C, the lowest temperature recorded there since 1975.

Abnormal low-elevation snowfalls occurred in Tasmania in early August. On 4 August, snow settled to sea level in Launceston in

Electric supply tower in Chubut, Argentina brought down by an intense snowstorm on 22 July 2020

Credit: Transpa S.A.

the city's most significant snowfall since 1921. Liawenee, in the central highlands, reached –14.2 °C on 7 August, a Tasmanian record low.

Significant cold weather affected parts of eastern Asia in the second half of December. Extremely heavy snow fell in parts of Japan as cold air of Siberian origin crossed the relatively warm waters of the Sea of Japan, with 19 sites, mostly on the Sea of Japan side of Honshu, setting records for 72-hour snowfall. There were major transport disruptions with many people stranded on roads for extended periods.

TROPICAL CYCLONES

The number of tropical cyclones globally was above average in 2020, with 98 named tropical storms in the 2020 northern hemisphere and 2019/2020 southern hemisphere seasons. The North Atlantic region had a very active season, with 30 tropical cyclones; this was more than double the long-term average and broke the record for a full season set in 2005. Most other basins had cyclone numbers near or slightly below average.

The accumulated cyclone energy (ACE) index, which integrates cyclone intensity and longevity, was well below average in all basins except the North Atlantic and North Indian Oceans, with the North-West Pacific about 50% below the long-term average. While ACE seasonal values for the North Atlantic were above average, they were well short of seasonal records.

The exceptionally active North Atlantic season resulted in a large number of landfalls. Twelve systems made landfall in the United States, breaking the previous record of nine, and five of those 12 systems made landfall in the state of Louisiana. The most severe impacts of the season in the United States came from Hurricane *Laura*, which reached category 4 intensity and made landfall on 27 August near Lake Charles in western Louisiana, leading to extensive wind and storm surge damage. *Laura* was also associated with extensive flood damage in Haiti and the Dominican Republic

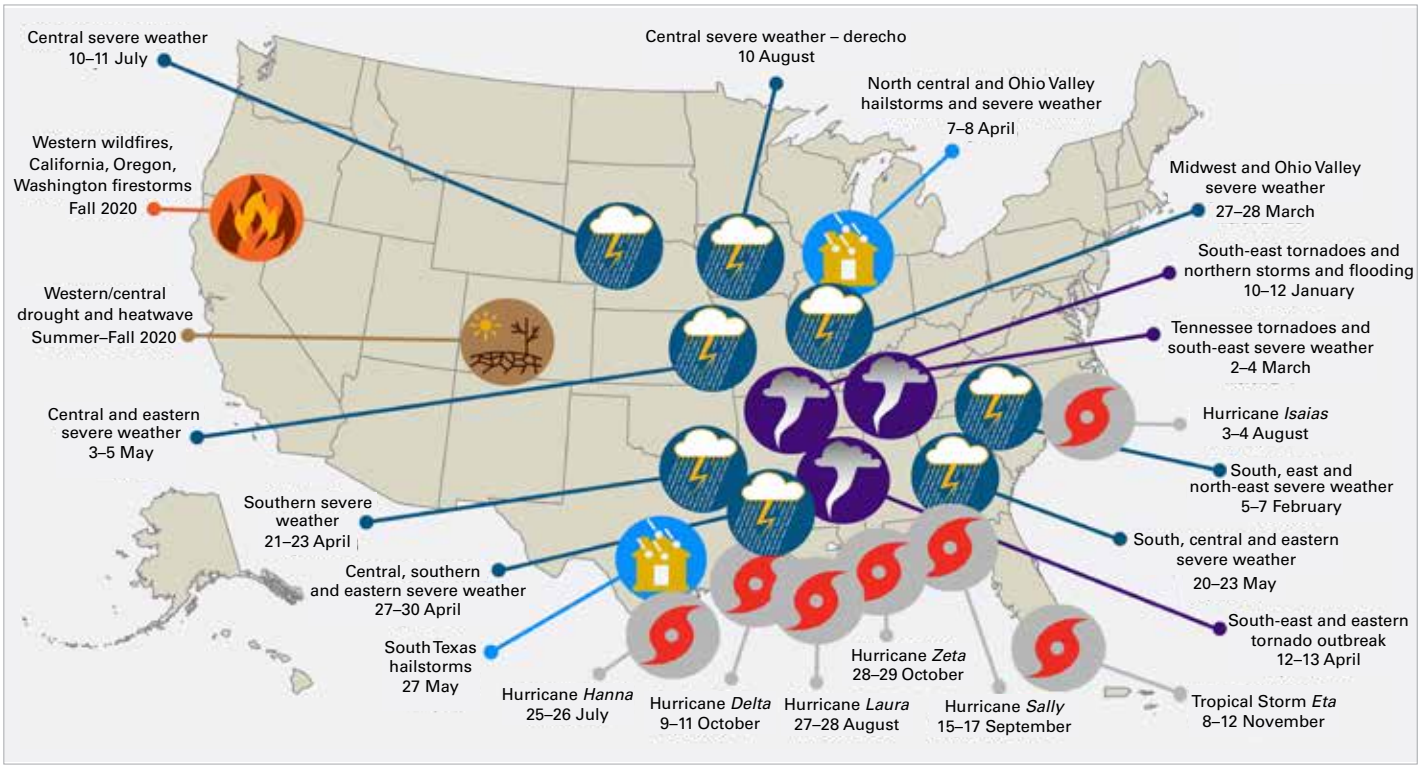

Figure 17. Billion-dollar weather and climate disasters affecting the United States in 2020. This map denotes the approximate location for each of the 22 separate billion-dollar weather and climate disasters that impacted the United States during 2020. *Source:* NOAA

in its developing phase. Seventy-seven deaths and US$ 19 billion in economic losses[41] were attributed to *Laura* across the three countries. Later in the season, two major hurricanes made landfall in rapid succession in Central America. Hurricane *Eta* made landfall as a category 4 system on the east coast of Nicaragua on 3 November, causing severe flooding in the region as it moved slowly across Nicaragua, Honduras and Guatemala. *Eta* moved offshore on 6 November and re-intensified to a tropical storm, making further landfalls in Cuba and the Florida Keys. Hurricane *Iota* was even stronger, becoming the season's first category 5 system off the Nicaraguan coast on 16 November. *Eta* and *Iota* also affected Colombia, and *Iota* was the first category 5 hurricane ever recorded so close to the Colombian national territory. Other damaging landfalls in the United States included those of Hurricane *Isaias* in North Carolina in August and Hurricane *Sally* in Alabama in September, while other parts of the region which experienced significant damage during the season included Bermuda, the Bahamas and the Yucatan Peninsula of Mexico.

Cyclone *Amphan*, which made landfall on 20 May near the India–Bangladesh border in the eastern Bay of Bengal, was the costliest tropical cyclone on record for the North Indian Ocean, with reported economic losses in India of approximately US$ 14 billion.[36] Large-scale evacuations of coastal areas in India and Bangladesh meant that casualties from *Amphan* were far lower than the number of casualties from previous comparable cyclones in the region. Nevertheless, 129 lives were lost across the two countries. *Amphan* reached category 5 intensity while over the Bay of Bengal, and although it weakened somewhat before landfall as a category 2 storm, it still led to extensive wind and storm surge damage in the city of Kolkata and surrounds. Later in the season, Cyclone *Gati* made landfall in north-eastern Somalia on 22 November, the first instance since satellite records began of a cyclone making landfall in Somalia at hurricane intensity.

The South-West Pacific experienced two category 5 cyclones in 2020. The first was Tropical Cyclone *Harold*, in April. Its most

[41] NCEI Billion-Dollar Weather and Climate Disasters database, https://www.ncdc.noaa.gov/billions/ (economic losses); EM-DAT, https://www.emdat.be/ (deaths)

significant impacts were in the northern islands of Vanuatu, where it made landfall at near peak intensity on 6 April. More than 17 000 homes were damaged or destroyed,[42] and about 65% of Vanuatu's population was affected,[43] with the city of Luganville among the hardest hit. There was significant damage in Fiji as *Harold* passed to the south of the main island of Viti Levu, while damage also occurred in Tonga and the Solomon Islands. Thirty deaths were reported along the cyclone's path, most of them when high seas washed passengers overboard from a ferry in the Solomon Islands. In December, Tropical Cyclone *Yasa* was one of the most intense cyclones ever recorded in the South-West Pacific, with a minimum central pressure of 899 hPa. Widespread damage occurred in Fiji, especially on the second largest island of Vanua Levu.

The strongest tropical cyclone of the season was Typhoon *Goni* (*Rolly*).[44] It crossed the northern Philippines on 1 November with a 10-minute mean wind speed of 220 km/h (or higher) at its initial landfall, making this one of the most intense landfalls on record. *Goni* (*Rolly*) was followed the next week by Typhoon *Vamco* (*Ulysses*), which was less intense but caused severe flooding in Manila and other areas. At least 25 deaths were attributed to *Goni* (*Rolly*) and 67 to *Vamco* (*Ulysses*).[45] Two major tropical cyclones hit the Korean Peninsula within a few days in early September, with Typhoon *Mayask* (*Julian*) making landfall near Busan on 3 September, followed by Typhoon *Haishen* (*Kristine*) on 7 September.

Mayask (*Julian*) brought 963.5 mm of rainfall over two days to a site on Jeju Island and brought wind gusts to the island of up to 177 km/h. Both tropical cyclones led to significant flooding on the Korean Peninsula and in western Japan, and 41 lives were lost when a ship sank off western Japan during the passage of *Maysak (Julian)*. Eight tropical cyclones and depressions made landfall in Viet Nam in less than five weeks in October and November, contributing to major flooding in the region.

Other tropical cyclones associated with significant loss of life through flooding were Cyclone *Diane* in Madagascar in January, and Tropical Storm *Amanda* in Guatemala and El Salvador in May.

EXTRATROPICAL STORMS

One of the costliest extreme events of the year was a fast-moving line of severe thunderstorms known as a derecho, which moved across the United States Midwest on 10 August, extending from South Dakota to Ohio. Iowa was the worst-affected area, with severe agricultural losses, including an estimated two million hectares of flattened corn and soybean crops. Over 90% of the buildings in the city of Cedar Rapids were damaged. Total losses were estimated at US$ 11 billion. The United States tornado season was below average, with the two most significant outbreaks affecting the Nashville area on 2–3 March and a broad area extending from Texas to Maryland on 12–13 April. Twenty-five lives were lost in the March outbreak and 35 in the April outbreak, with losses of several billion dollars across the two events.[46]

Severe thunderstorms affected a wide area of eastern Australia during the third week of January. The most significant damage was in Canberra, where hail 5 cm in diameter on 20 January led to extensive vehicle and building damage across a broad swathe of the city. Significant hail damage also occurred in some eastern suburbs of Melbourne. Total losses from the storms were estimated at

[42] Australian Department of Foreign Affairs and Trade, https://www.dfat.gov.au/crisis-hub/Pages/tropical-cyclone-harold.

[43] FAO, http://www.fao.org/resilience/resources/resources-detail/en/c/1274007/

[44] Names in parentheses are alternative local names for the storms.

[45] Philippines National Disaster Risk Reduction and Management Council, situational reports

[46] All impact assessments in this paragraph are taken from the NCEI Billion-Dollar Weather and Climate Disasters database. https://www.ncdc.noaa.gov/billions/.

US$ 1.1 billion.[47] Further major hailstorms affected Queensland on 31 October, with hailstones as large as 14 cm in diameter reported in the suburbs of Brisbane. Other major severe storms included a hailstorm in Calgary (Canada) on 13 June, with insured losses exceeding US$ 1 billion, a squall line which crossed southern Brazil on 30 June, with tornadoes, hail and wind gusts exceeding 100 km/h and 12 associated deaths, and a hailstorm in Tripoli (Libya) on 27 October, with hailstones as large as 20 cm accompanied by unusually cold conditions.

A number of severe extratropical cyclones affected northern, central and western Europe in February, contributing to a very wet month with flooding in some areas.[48] The most significant storm of this period was *Ciara* (also known as *Sabine* and *Elsa*), which passed to the north-west of Europe on 10–11 February. Significant wind damage extended from Ireland to Sweden, Poland and Italy. In the autumn, Storm *Alex* in early October brought extreme winds to western France, with gusts as high as 186 km/h and heavy rain over a wide area. 3 October was the wettest area-averaged day on record for the United Kingdom of Great Britain and Northern Ireland, with a national average of 31.7 mm, while extreme rainfall occurred near the Mediterranean coast on both sides of the France–Italy border, with 24-hour totals exceeding 600 mm in Italy and 500 mm in France. The extreme rainfall extended to southern Switzerland, where 421 mm fell in 24 hours at Càmedo. Significant flash flooding occurred in all three countries. A Mediterranean cyclone hybrid system ("Medicane"), showing some characteristics of a tropical cyclone and others of a mid-latitude storm, developed in mid-September, making landfall in south-western Greece on 18 September with wind gusts exceeding 110 km/h. Earlier, it brought heavy rainfall and flash flooding to coastal Libya, with a daily rainfall total of 150.5 mm at Sabratha on 15 September.

[47] Insurance Council of Australia, media release of 27 August 2020

[48] Austria contribution, Bosnia and Herzegovina contribution

Climate indicators and sustainable development goals

The 2030 Agenda for Sustainable Development provides a shared blueprint for peace and prosperity for people and the planet, now and into the future. At its heart is a set of sustainable development goals (SDGs), which recognize that ending poverty and other deprivations must go hand-in-hand with strategies that improve health and education, reduce inequality, and spur economic growth, while tackling climate change and preserving oceans and forests. The achievement of many of these goals is put at risk by climate change, however. For example, rising temperatures are leading to the loss of species and ecosystems, which can reduce agricultural and fishing yields, contributing to food insecurity and affecting livelihoods (SDGs 1, 2, 14 and 15). Extreme weather and climate events can increase health risks, damage infrastructure and lead to water scarcity (SDGs 1, 3, 6, 9 and 11). These threats, together with others, are interrelated with conflict and stability (SDG 16). Uneven distribution of such risks across populations and regions can reinforce or worsen existing inequalities (SDG 10).

Figure 18 demonstrates how rising atmospheric CO_2 concentrations lead to cascading effects via six of the other key climate indicators. Beyond posing risks to achieving sustainable development, some of these processes also have the potential to release further greenhouse gases into the atmosphere in a feedback loop that can perpetuate warming. For example, rising temperatures can thaw permafrost, releasing more carbon into the atmosphere.

International Committee of the Red Cross, 2020: *When rain turns to dust: Understanding and responding to the combined impact of armed conflicts and the climate and environment crisis on people's lives*, https://www.icrc.org/sites/default/files/topic/file_plus_list/rain_turns_to_dust_climate_change_conflict.pdf.

Intergovernmental Panel on Climate Change, 2014: *AR5 Synthesis Report: Climate Change 2014*, https://www.ipcc.ch/report/ar5/syr/

Trewin, B., et al., 2021: Headline Indicators for Global Climate Monitoring. *Bulletin of the American Meteorological Society*, 102(1): E20–E37, https://doi.org/10.1175/BAMS-D-19-0196.1.

World Meteorological Organization, 2020: *WMO Statement on the State of the Global Climate in 2019*, https://library.wmo.int/index.php?lvl=notice_display&id=21700.

United Nations Sustainable Development Goals, https://sdgs.un.org/goals.

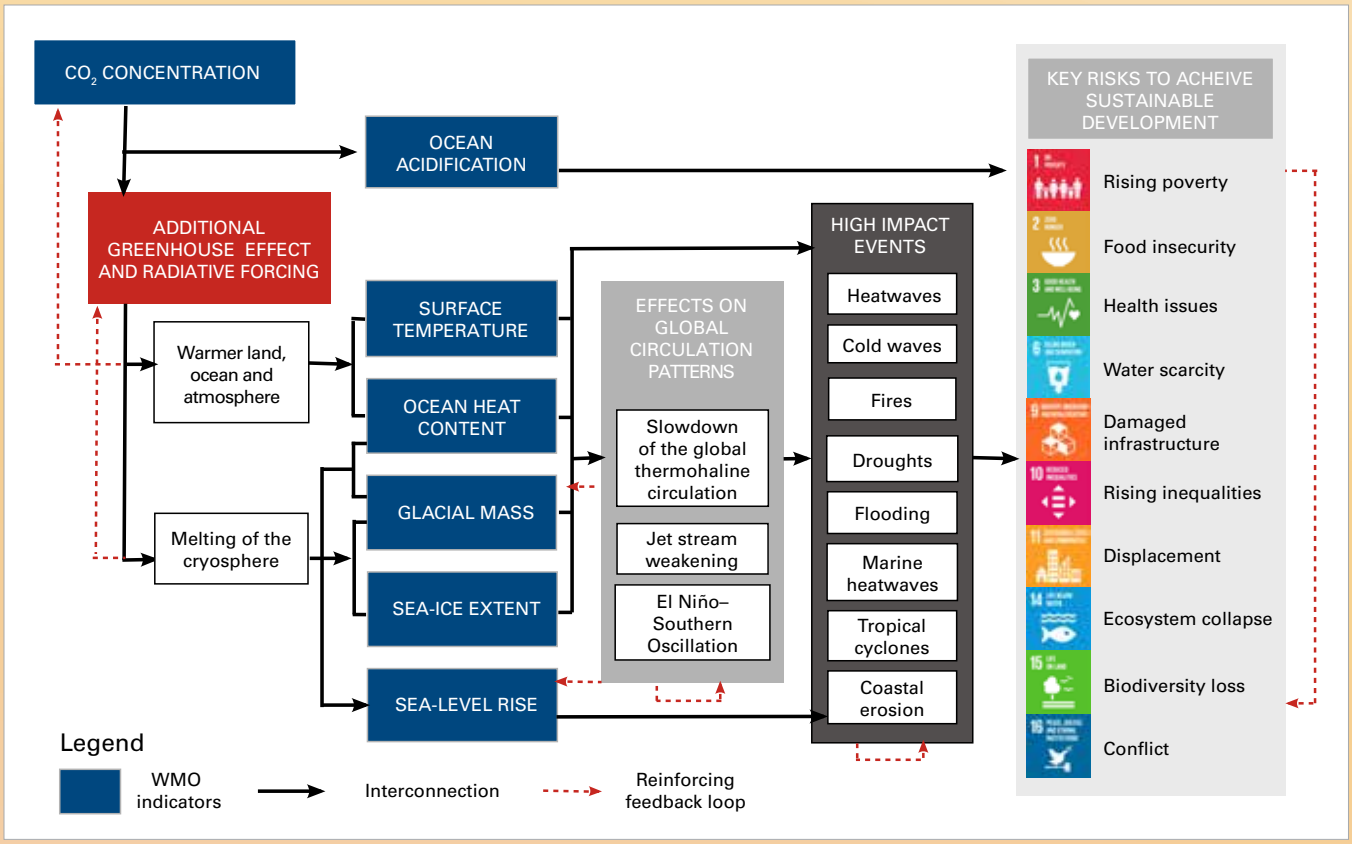

Figure 18. Selected climate change-related risks to the achievement of the SDGs

Observational basis for climate monitoring

Climate monitoring is performed by a system of observing systems covering the atmosphere, the ocean, hydrology, the cryosphere and the biosphere. Each of these areas is monitored in different ways by a range of organizations. Cutting across all these areas, satellite observations provide major contributions to global climate monitoring.

In 1992, the Global Climate Observing System (GCOS) was established by WMO, the Intergovernmental Oceanographic Commission (IOC) of the United Nations Educational, Scientific and Cultural Organization (UNESCO), the United Nations Environment Programme (UNEP) and the International Science Council (ISC) to coordinate and facilitate the development and improvement of global climate observations. GCOS has identified a set of Essential Climate Variables (ECVs) that together provide the information necessary to understand, model and predict the trajectory of the climate as well as plan mitigation and adaptation strategies (Figure 19). The status of the observational basis for these ECVs is published in regular status reports. GCOS also identifies what is needed to improve the system in implementation reports.

In addition to observations provided by the GCOS-coordinated Global Surface Network (GSN) and Global Upper-Air Network (GUAN), National Meteorological and Hydrological Services (NMHSs) of WMO Members provide a more comprehensive and widespread network of observation, acquired primarily for operational weather prediction. WMO's Global Basic Observing Network (GBON), a globally designed network with prescribed capabilities and observing schedules and for which international data exchange is mandatory, will provide critically needed observations for numerical weather prediction and will help substantially strengthen climate monitoring.

In order to provide the necessary financial and technical assistance for the implementation and operation of GBON in the poorest and most poorly observed areas of the globe, WMO and the members of the Alliance for

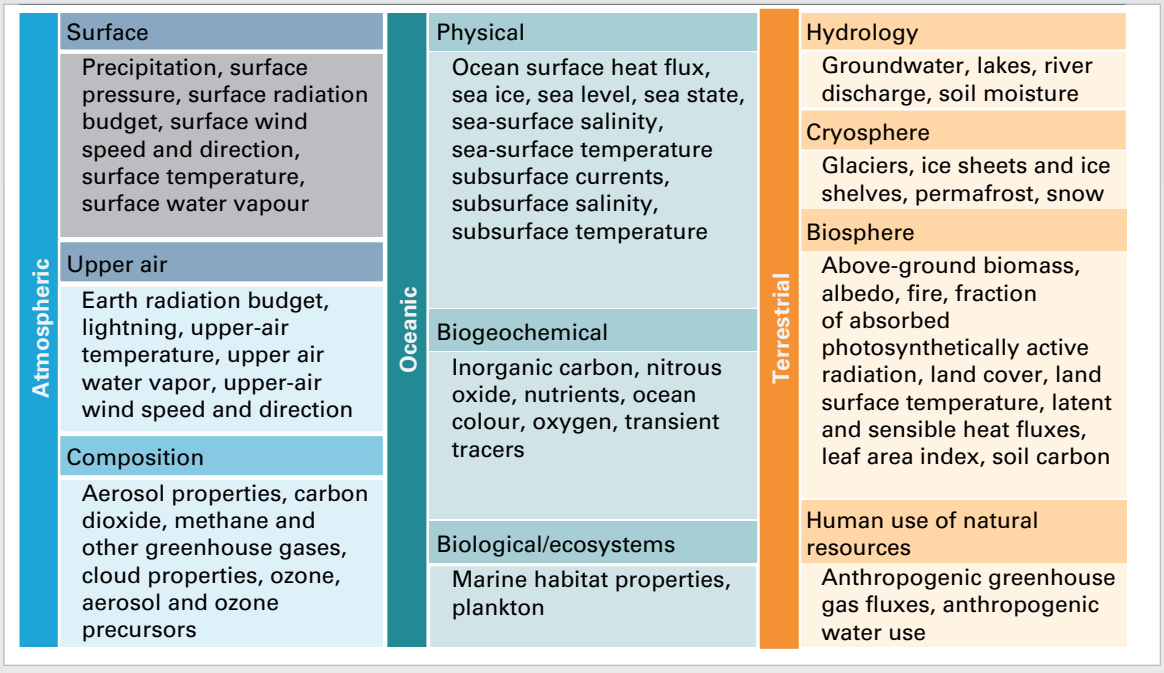

Figure 19. Essential Climate Variables (ECVs) identified by GCOS

Hydromet Development[a] are establishing a Systematic Observations Financing Facility (SOFF).

Complementing the observations of the physical and dynamic properties of the atmosphere, WMO's Global Atmospheric Watch (GAW) coordinates atmospheric composition measurements, ensuring that reliable and accurate data are obtained from measurements made by WMO Members, research institutions and/or agencies and other contributing networks.

Ocean observations of ocean physics, biogeochemistry, biology and ecosystems are coordinated through the Global Ocean Observing System (GOOS). The GOOS Observations Coordination Group (OCG) monitors the performance of these observations[b] and produces an annual Ocean Observing System Report Card. Ocean observations are generally made widely available to international users.

In the terrestrial domain, there is a wider group of observing networks. Hydrological observations are generally operated by NMHSs and coordinated through WMO. A number of specialized Global Terrestrial Networks (GTNs), for example, on hydrology, permafrost, glaciers, land use, and biomass, also report to GCOS. Data exchange agreements are generally less developed for the terrestrial networks, and many important observations are not made available to international users.

The Committee on Earth Observation Satellites/Coordination Group for Meteorological Satellites (CEOS/CGMS) Joint Working Group on Climate (WGClimate) bases the development of satellite observations for climate on the ECV requirements established by GCOS. It has produced an ECV Inventory that includes records for 766 climate data records for 33 ECVs covering 72 separate ECV products, with more planned. Satellite observations have some advantages – they have near-global coverage – but optical observations can be interrupted by clouds. Used with ground-based observations, either as complementary data sets, or for validation and calibration, they form an invaluable part of the global observing system.

Monitoring the climate system from space: A very large-scale sand plume observed on 23 June 2020, transporting billions of tons of sand from the African desert across the Atlantic, illustrating interlinkages of the climate system across the continents

[a] https://public.wmo.int/en/our-mandate/how-we-do-it/partnerships/wmo-office-of-development-partnerships

[b] https://www.ocean-ops.org/

Risks and impacts

The risk of climate-related impacts depends on complex interactions between climate-related hazards and the vulnerability, exposure and adaptive capacity of human and natural systems. At current levels of global greenhouse gas emissions, the world remains on course to exceed the agreed temperature thresholds of either 1.5 °C or 2 °C above pre-industrial levels, which would increase the risks of pervasive climate change impacts beyond what is already seen.

Climate-related events already pose risks to society through impacts on health, food and water security, as well as human security, livelihoods, economies, infrastructure and biodiversity. Climate change also has implications for ecosystem services. It can affect patterns of natural resource use, as well as the distribution of resources across regions and within countries.

Climate change and individual climate-related events have significant environmental repercussions as well. Negative environmental effects include impacts to the land, such as droughts, wildfires in forest and peatland areas, land degradation, sand and dust storms, and desertification. Air pollution is linked to the use of fossil fuels. In freshwater systems, impacts include floods and water stress, and in marine systems, they include sea-level rise, ocean acidification, reduced levels of ocean oxygen, mangrove decay and coral bleaching. Many of these impacts are linked to biodiversity loss. For example, besides the heavy human impacts of the wildfires in Australia in 2019 and early 2020, there was likely a severe loss or displacement of many millions of animals during the disaster.[49]

In 2020, the COVID-19 pandemic had wide-ranging impacts on health and well-being, livelihoods, businesses and economies across the world. While countries and communities worldwide responded to the specific risks and impacts of the pandemic, the risks associated with other hazardous events did not go away. During the course of 2020, countries and communities also prepared for and responded to seasonal and emerging extreme weather events, other natural hazards and outbreaks of diseases taking into account the COVID-19 situation in each country/community and incorporating additional precautions for a safe response to the pandemic. WHO, in collaboration with WMO, issued a WHO health advisory to provide guidance on adapting preparedness and response plans and procedures for cyclones, tropical storms, tornadoes, floods, earthquakes and potential outbreaks of other diseases to their COVID-19 strategic preparedness and response plans.[50] The WHO advisory reinforces the application of risk-based and whole-of-society approaches as laid out in the WHO Health Emergency and Disaster Risk Management Framework,[51] the critical roles of stakeholders from community, national and international levels, and the collaboration among hydrometeorological, health and disaster management organizations, as well as the implementation of the International Health Regulations (2005).[52]

HUMAN MOBILITY AND DISPLACEMENT

Climate and weather events had major and diverse impacts on population movements and on the vulnerability of people on the move throughout 2020. In line with previously reported patterns, many of the largest scale displacements were in populous Asian countries. Furthermore, the complexity of human-mobility-related risks and impacts tends to be greatest – and least understood due to major limitations with respect to the available data – in relation to slow-onset events and in fragile and conflict-affected contexts; knowledge in this area is relevant

[49] https://www.aph.gov.au/About_Parliament/Parliamentary_Departments/Parliamentary_Library/pubs/rp/rp1920/Quick_Guides/AustralianBushfires

[50] World Health Organization, 2020: *Preparedness for cyclones, tropical storms, tornadoes, floods and earthquakes during the COVID-19 pandemic: health advisory, 29 April 2020*, https://apps.who.int/iris/handle/10665/332408

[51] World Health Organization, 2019: *Health emergency and disaster risk management framework*, https://apps.who.int/iris/handle/10665/326106

[52] World Health Organization, 2016: International Health Regulations (2005), 3rd ed.,https://apps.who.int/iris/handle/10665/246107

for global and national policy development, operations and research in the domains of human mobility and climate action. In 2020, the COVID-19 pandemic added a further dimension to human mobility concerns, highlighting the need for an integrated approach to understanding and addressing climate risk and impacts on vulnerable populations.

Dust storm in Polatlı, Ankara, 12 September 2020.
Source: State of the Climate in Turkey in 2020

WEATHER AND CLIMATE-RELATED HAZARDS AND DISASTERS DRIVING NEW DISPLACEMENT

Over the past decade (2010–2019), weather-related events triggered an estimated 23.1 million displacements of people on average each year.[53] The overwhelming majority of weather-related displacements take place within national borders, though cross-border movements may also occur. Some 9.8 million displacements, largely due to hydrometeorological hazards and disasters, were recorded during the first half of 2020, mainly concentrated in South and South-East Asia and the Horn of Africa.[54] Events in the second half of the year, including displacements linked to flooding across the Sahel region, the active Atlantic hurricane season and typhoon impacts in South-East Asia, are expected to bring the total for the year close to the average for the decade.

In May, Cyclone *Amphan* hit the Sundarbans region between India and Bangladesh. 2.4 million people were displaced in India, mostly in West Bengal and Odisha, and 2.5 million were displaced in Bangladesh. While many returned relatively soon afterwards, damage to more than 2.8 million homes likely resulted in homelessness and prolonged displacement for many thousands.[77] Many displaced people did not have access to evacuation centres and were compelled to take shelter in tents or in the open air on embankments.[78]

Monsoon rains led to massive flooding, dam collapses, landslides, and the displacement of millions of people in Bangladesh, China, India, Japan, Pakistan,[55] Nepal,[56] the Republic of Korea,[57] Turkey[58] and Viet Nam. The floods and landslides in China were particularly intense. 29 000 homes were destroyed, and over 2.2 million people were evacuated by mid-July 2020.[59]

In July, flooding and landslides affected several districts across Nepal. International Organization for Migration (IOM) assessments in August showed the presence of a total of 5 467 persons from 1 066 households in 29 displacement sites across the country.[60] By September, only 12 sites were still active, hosting some 2 000 individuals in three districts, as people returned home with the end of the monsoon season.[61]

---

[53] Data sourced from the Internal Displacement Monitoring Centre's Global Internal Displacement Database (GIDD).

[54] IDMC, Internal displacement 2020: Mid-year update

[55] http://floodlist.com/asia/pakistan-glof-golen-valley-chitral-july-2020

[56] https://www.aljazeera.com/videos/2020/07/25/south-asia-monsoon-more-than-130-people-killed-in-nepal-floods/

[57] http://floodlist.com/asia/south-korea-flash-floods-july-2020

[58] http://floodlist.com/asia/turkey-rize-floods-july-2020

[59] Xinhua Net, China increases disaster relief funds amid floods, 13 July 2020, http://www.xinhuanet.com/english/2020-07/13/c_139209865.htm.

[60] https://dtm.iom.int/reports/nepal-%E2%80%93-landslides-and-floods-displacement-%E2%80%93-site-assessment-report-september-2020

[61] https://dtm.iom.int/reports/nepal-%E2%80%93-landslides-and-floods-displacement-%E2%80%93-site-assessment-round-2-october-2020

Philippine Red Cross teams performed rescue operations after debris from Super Typhoon *Goni* caused the Magnus River to overflow, which resulted in flooding.

Credit: Philippine Red Cross

In the Philippines, Super Typhoon *Goni* (locally known as *Rolly*) displaced 400 000 people when it made landfall across the country on 1 November.[62] Two weeks later, Typhoon *Vamco* triggered a further 320 000 displacements.[63] In October 2020, Cyclone *Molave*, the fourth storm of the month to hit Viet Nam, triggered the evacuation of some 1.3 million people and left hundreds of thousands of people in a critical situation as crops were destroyed.[64]

2020 also saw some of the largest wildfires on record, which led to significant displacement. The 2020 fire season in the USA resulted in the destruction of at least 2 000 residential buildings in California and displaced some 100 000 people. In Oregon, around 500 000 people were placed under evacuation notice, and more than 40 000 had to be evacuated from their homes.[65] In Australia, around 65 000 new displacements were recorded as a consequence of the fires that affected the country between July 2019 and February 2020. Fires also destroyed 3 100 homes in Australia, potentially leading to longer-term displacement of some 8 100 people.[66]

PATTERNS OF PROTRACTED, PROLONGED AND REPEATED DISPLACEMENT LINKED WITH HYDROMETEOROLOGICAL HAZARDS

Many displacement situations triggered by hydrometeorological events have become prolonged or protracted for people unable to return to their former homes or without options for integrating locally or settling

[62] https://disasterphilanthropy.org/disaster/super-typhoon-goni/, https://www.voanews.com/east-asia-pacific/aid-groups-urge-assistance-after-super-typhoon-goni-hits-philippines, https://reliefweb.int/sites/reliefweb.int/files/resources/Philippines%20-%20Typhoon%20Goni%20-%20Flash%20Update%20No.%201%20(as%20of%2031%20October%202020,%209%20p.m.%20local%20time).pdf

[63] https://www.thenewhumanitarian.org/maps-and-graphics/2020/11/16/typhoon-vamco-philippines-vietnam-flooding-climate-change

[64] https://media.ifrc.org/ifrc/press-release/homes-1-million-people-ruin-major-typhoon-hits-viet-nam/

[65] https://storymaps.arcgis.com/stories/064d9b11d0584625ba57b172612699c1

[66] https://www.internal-displacement.org/sites/default/files/publications/documents/Australian%20bushfires_Final.pdf

elsewhere. While several storms and floods led to damage in Mozambique in 2020, over a year after cyclones *Kenneth* and *Idai* hit the country in March and April 2019, tens of thousands of people remain displaced and held back from recovery.[67] An assessment conducted in October 2020 identified 93 324 people still displaced in the country's central region (of whom 81 251 were displaced by *Idai* and 12 073 by the 2020 floods).[68] In Cabo Delgado, almost 6 500 internally displaced people were staying in displacement sites.[69]

Due to the continuing or growing risk in their areas of origin (and return) or settlement, people who have been displaced by hydrometeorological and climatic events may also be subject to repeated and frequent displacement, leaving little time for recovery between one shock and the next. This has implications for disaster preparedness and management and also for supporting solutions to displacement that are sustainable and supporting the resilience of people who might otherwise see their living conditions progressively eroded through repeated disasters and displacement.

COMPOUNDED RISK AND VULNERABILITY

Refugees, internally displaced people and migrants are often among those most vulnerable to climate- and weather-related hazards. Many vulnerable people on the move, regardless of their reasons for moving, end up settling in high risk areas, where they are exposed to climate and weather hazards at a range of scales. Weather hazards and human mobility may also intersect with social and political tensions and conflict in complex settings and, as such, require the integrated consideration of multi-hazard disaster risk reduction measures, including early warning systems and preparedness, and longer-term sustainable development concerns, such as land use and urban planning.

Specific conditions of risk from hydrometeorological disasters are particularly well documented in the Rohingya refugee sites in Cox's Bazar, Bangladesh. Over the year, a total of 162 275 people were affected, with many requiring specific assistance.[70] Without preparedness measures undertaken in the camp areas, including kits for strengthening shelters, building of retaining structures on hillsides, and improving drainage, roads and bridges, these impacts would have been worse.[71]

In East Africa, floods and the worst desert locust infestation in 25 years resulted in large-scale displacement. In Somalia, floods were associated with the displacement of over one million people in 2020, mostly inside the country, while drought-related impacts induced a further 80 000 displacements.[72,73] Around a quarter of the population affected by floods in 2020 consisted of people already living in overcrowded and insecure camps for internally displaced people,[74] to which many newly flood-displaced people also moved.[75]

---

[67] UNHCR, https://www.unhcr.org/news/stories/2020/3/5e6a6e50b/year-people-displaced-cyclone-idai-struggle-rebuild.html

[68] https://displacement.iom.int/reports/mozambique-%E2%80%93-covid-19-preparedness-assessment-resettlement-sites-report-12-october-2020

[69] https://reliefweb.int/report/mozambique/rapid-response-plan-cabo-delgado-province-mozambique-may-december-2020, https://dtm.iom.int/reports/mozambique-%E2%80%93-covid-19-preparedness-assessment-resettlement-sites-cabo-delgado-and-nampula

[70] https://www.arcgis.com/apps/MapSeries/index.html?appid=1eec7ad29df742938b6470d77c26575a

[71] UNHCR, https://www.unhcr.org/refugeebrief/the-refugee-brief-22-may-2020/

[72] UNHCR Somalia Factsheet September 2020, https://data2.unhcr.org/en/documents/details/83089

[73] Executive Committee of the High Commissioner's Programme, *Update on UNHCR's operations in the East and Horn of Africa and the Great Lakes, 29 September 2020*, Seventy-first session, 5-9 October 2020, https://www.unhcr.org/5f734d884.pdf

[74] IDMC, Disasters meet political unrest, displacing millions in East Africa, July 2020, https://www.internal-displacement.org/expert-opinion/disasters-meet-political-unrest-displacing-millions-in-east-africa

[75] Executive Committee of the High Commissioner's Programme, *Update on UNHCR's operations in the East and Horn of Africa and the Great Lakes, 29 September 2020*, Seventy-first session, 5-9 October 2020, https://www.unhcr.org/5f734d884.pdf and UNHCR briefing note on Somalia

Farmers whose crops were devastated by desert locusts were also forced to move in search of survival assistance.[76]

In Ethiopia, over 300 000 displacements, two thirds of which were in the Somali region, were brought on by floods and landslides during the first half of the year.[77] IOM assessments between June and July 2020 determined that at least 104 696 people were displaced by floods and 351 062 by droughts in the country's south-east – respectively 6% and 19% of the local displaced population.

Sudan experienced flash floods, and rivers, including the Nile, overflowed in August 2020. Some 125 000 refugees and internally displaced people were among those affected.[78]

Between August and September 2020, extreme rainfall triggered floods that struck several countries in the Sahel. IOM assessments estimated a total of 1.25 million people displaced in Burkina Faso, Mali and Niger – in contexts already characterized by conflict and food insecurity, as well as forced internal and cross-border population movements. The further degradation of living conditions and livelihoods resulting from the floods increased the risk of displacement within the region, southward to coastal countries and northward to North Africa and Europe.[79] Floods in August 2020 in N'Djamena, Chad, resulted in 31 853 individuals fleeing their homes and finding shelter elsewhere in the city, with little relief assistance being provided. Floods also affected the Lac province, displacing over 4 000 people and affecting many more who had previously been displaced by conflict and violence.[80]

In Yemen – where more than 80% of the total population is in need of humanitarian assistance – severe flash floods displaced many who were already internally displaced because of the conflict, living in conditions of abject poverty and in precarious shelters without access to secure alternatives. Some 300 000 people lost their homes, crops, livestock and belongings due to rain and floods. The sudden breaching of the Al-Roone dam affected thousands of people in internally displaced person sites in Al-Tahseen, Souq al-Lill and elsewhere.[81]

In Syria, from early October, wildfires in Lattakia, Tartous and Homs affected up to 40 000 people through damage to housing and assets and major loss of livelihoods. Some 25 000 displacements were reported, including from areas with recently returned internally displaced people. The resilience of affected communities has been eroded over 10 years of conflict, as well as by the COVID-19 pandemic, economic crises and the preceding massive uptake of displaced people.[82]

COMPOUNDED CRISIS IMPACTS ON FOOD SECURITY, DISPLACEMENT, AND HUMANITARIAN ACTION

After decades of decline, the recent increase in food insecurity since 2014 is being driven by conflict and economic slowdown as well as climate variability and extreme weather events. Nearly 690 million people, or 9% of the world population, were undernourished, and about 750 million, or nearly 10%, were exposed to severe levels of food insecurity

---

[76] IDMC, Internal Displacement 2020: Mid-year Update, https://www.internal-displacement.org/publications/internal-displacement-2020-mid-year-update

[77] United Nations Office for the Coordination of Humanitarian Affairs, *Ethiopia Floods Response Plan, Belg/Gu Season Floods (May 2020*), https://reliefweb.int/report/ethiopia/ethiopia-floods-response-plan-belggu-season-floods-may-2020

[78] UNHCR, Massive floods in Sudan impact thousands of refugees, 24 September 2020, https://www.unhcr.org/news/stories/2020/9/5f6c42834/massive-floods-sudan-impact-thousands-refugees.html

[79] UNHCR Sahel Crisis Response Progress Report: Responding to the urgent needs of refugees, internally displaced, returnees and others of concern, January-September 2020, https://reporting.unhcr.org/sites/default/files/UNHCR%20Sahel%20Appeal%20-%20Progress%20Report%20-%20January%20to%20September%202020%20.pdf

[80] https://dtm.iom.int/chad, https://reliefweb.int/disaster/fl-2020-000192-tcd

[81] UNHCR, *300,000 people lose homes, incomes, food supplies and belongings due to catastrophic flooding in Yemen*, 21 August 2020, https://www.unhcr.org/news/briefing/2020/8/5f3e7faf4.html

[82] https://reliefweb.int/sites/reliefweb.int/files/resources/MDRSY005do.pdf

in 2019[83] (Figure 20). The number of people classified under crisis, emergency and famine conditions (Integrated Food Security Phase Classification 3 or above) had increased to almost 135 million people across 55 countries.[84]

In 2020, over 50 million people were doubly hit – by climate-related disasters (floods, droughts and storms) and by the COVID-19 pandemic.[85] Countries in Central America suffered from the triple-impact of Hurricanes *Eta* and *Iota*, COVID-19 and pre-existing humanitarian crises. The Government of Honduras estimated that 2.8 million people were affected by Hurricane *Eta*, and 53 000 hectares of cropland, mainly rice, beans, and sugarcane, were washed away.[86] Among the Pacific Islands, Tropical Cyclone *Harold* affected over 17 500 hectares of cropland in Vanuatu, causing substantial damage just as the growing season began.[87] (For more information about Tropical Cyclone *Harold*, see Tropical Cyclones.) The long period of dry weather already observed in South America in 2020 is likely to continue as La Niña often brings below-average precipitation to some areas. As a result, corn production in Argentina is forecast to drop by 2 million tons (a 5% decline) in 2020–2021.[88]

The restrictions to prevent the spread of COVID-19, particularly measures to limit the movement of people within and between countries and the sale and purchase of goods and services, have posed significant challenges for managing the impacts of climate-related disasters on food insecurity. The feasibility of face-to-face services to provide farmers with information from seasonal weather forecasts as guidance on early actions has been reduced in many countries.[89] Disruptions to the agriculture sector by COVID-19 have

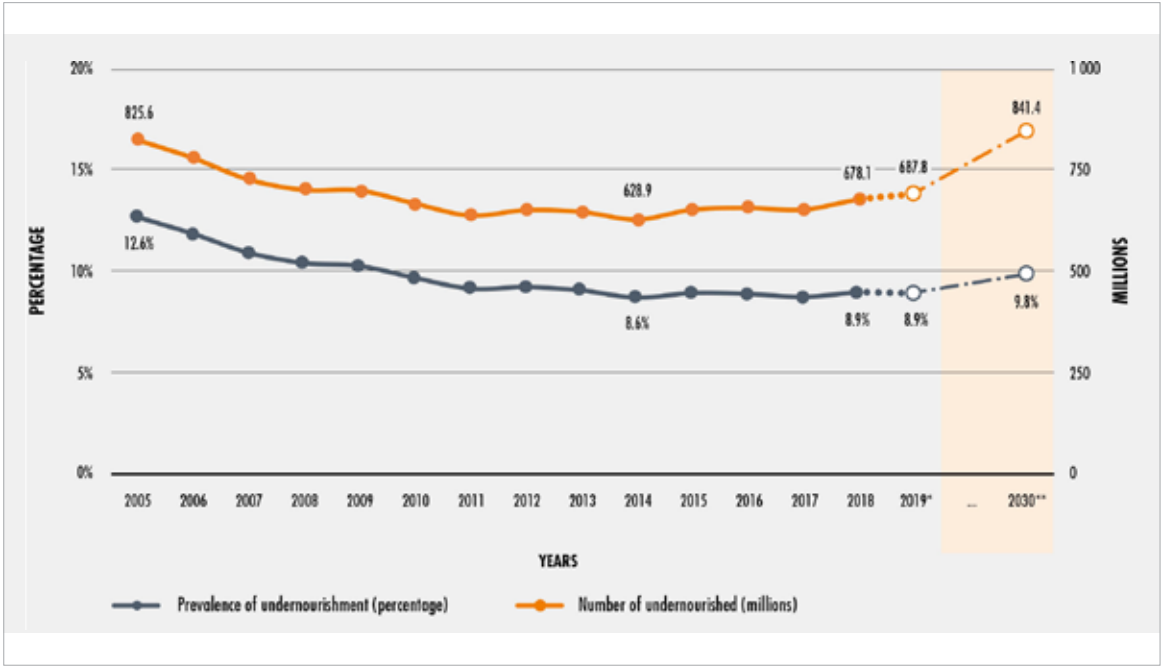

Figure 20. The number of undernourished people in the world continued to increase in 2019. Projected values in the figure are illustrated by dotted lines and empty circles. The entire series has been revised to reflect the latest information and replaces all series published previously.
Source: Food and Agriculture Organization of the United Nations (FAO)

[83] Food and Agriculture Organization of the United Nations, 2020: *The State of Food Security and Nutrition in the World 2020. Transforming food systems for affordable healthy diets*, http://www.fao.org/3/ca9692en/online/ca9692en.html

[84] 2020-Global report on food crisis. https://docs.wfp.org/api/documents/WFP-0000114546/download/

[85] International Federation of Red Cross and Red Crescent Societies: https://media.ifrc.org/ifrc/wp-content/uploads/2020/11/20201116_WorldDisasters_Full.pdf

[86] COPECO 2020. Reporte de estadísticas de incidente causados por el Huracán ETA, https://sigmof.icf.gob.hn/?page_id=7426

[87] The Pacific Islands: Tropical Cyclone Harold. Situation report-May 2020

[88] United States Department of Agriculture, World Agricultural Production report, https://apps.fas.usda.gov/psdonline/circulars/production.pdf

[89] Food and Agriculture Organization of the United Nations, 2020: *The dual threat of extreme weather and the COVID-19 crisis: Anticipating the impacts on food availability*, http://www.fao.org/documents/card/en/c/cb0206en

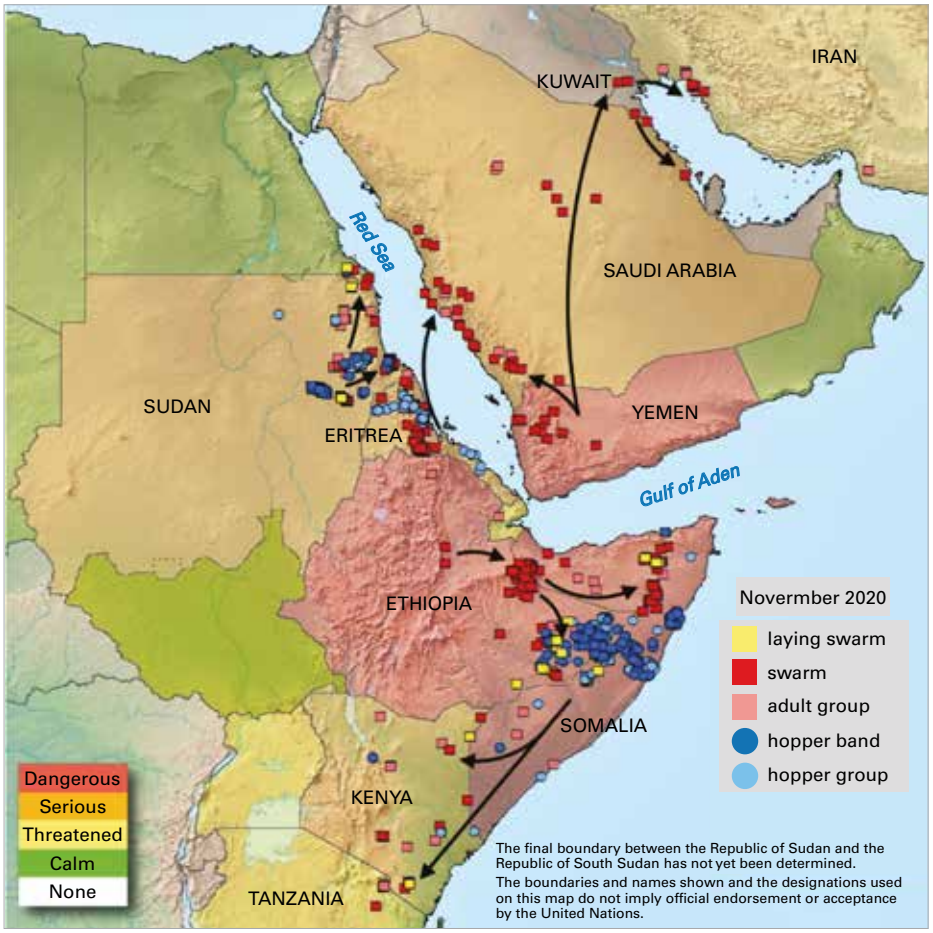

Figure 21. Desert locust movement prediction using FAO´s Desert Locust Information System (DLIS). The unusual weather conditions in autumn 2019 along the Arabian Peninsula generated strong cyclones and heavy rains, resulting in higher-than-normal vegetation growth, which provided ideal conditions for desert locusts. During the multiple crises in 2020, early warnings and early action responses played a key role in saving up to 3.1 million tons of cereals (enough to feed 18 million people in one year), worth around US$ 800 million, across nine eastern African countries and Yemen. *Source:* Food and Agriculture Organization of the United Nations, 2020: *Desert locust upsurge – Progress report on the response in the Greater Horn of Africa and Yemen (May–August 2020)*, http://www.fao.org/3/cb1500en/cb1500en.pdf; Food and Agriculture Organization of the United Nations, 2020: *Early Warning Early Action Report on food security and agriculture (April–June 2020)*, http://www.fao.org/3/ca8606en/CA8606EN.pdf

exacerbated weather impacts along the entire food supply chain, elevating levels of food insecurity, malnutrition and undernourishment.

The largest desert locust outbreak in 25 years in the Greater Horn of Africa and Yemen, triggered by heavy rains, has exacerbated existing conditions of undernourishment, and efforts to combat this outbreak have been disrupted by restrictions on the movement of personnel and disruptions in the supply chain of equipment due to the pandemic. In Ethiopia alone, 200 000 hectares of cropland were damaged, and over 356 000 tons of cereals were lost, leaving almost one million people food insecure.[90] By September 2020, data suggested that the number of Somalis facing acute malnutrition (Integrated Food Security Phase Classification (IPC) Phase 3 or above) and marginally able to meet minimum food needs tripled to 3.5 million compared to early 2020.[91] Desert locusts and river floods were responsible for crop losses within the country, with an estimated reduction in cereal production of 1 525% during the April–June growing season (Figure 21).[92]

COVID-19 IMPACTS ON HUMANITARIAN ACTION

Mobility restrictions and economic downturns due to COVID-19 have slowed the delivery of humanitarian assistance to vulnerable people on the move as well as efforts to support recovery for affected persons, including

[90] FAO in Ethiopia, http://www.fao.org/ethiopia/news/detail-events/en/c/1270924/

[91] Food Security and Nutrition Analysis Unit - Somalia. Food Security and Nutrition Quarterly Brief May 2020, https://www.fsnau.org/node/1756

[92] Somalia Food Security Outlook, https://fews.net/, https://fews.net/east-africa/somalia/food-security-outlook-update/april-2020

durable solutions for those displaced. The vulnerabilities of displaced populations, which often live in densely populated settlements, were amplified further.[93]

Cyclone *Harold*, which struck Fiji, the Solomon Islands, Tonga and Vanuatu and was one of the strongest storms ever recorded in the South Pacific,[94] triggered an estimated 99 500 displacements. Because of COVID-19 lockdowns and quarantines, response and recovery operations were hampered leading to delays in providing equipment and assistance.[95]

Likewise, in the Philippines, the pandemic complicated evacuation and response efforts ahead of Tropical Cyclone *Vongfong* (*Ambo*) in mid-May. Over 180 000 people were pre-emptively evacuated,[96] though operations were hampered by the need for social distancing measures as residents could not be transported in large numbers and evacuation centres could only be used at half capacity.[97] The storm also damaged Bicol Region's only COVID-19 testing facility.[98]

In northern Central America, some 5.3 million people were in need of humanitarian assistance, including 560 000 internally displaced people before the onset of the pandemic.[99] Responses to storms and cyclones that repeatedly affected the area throughout the Atlantic hurricane season therefore took place in the context of complex, interlinked vulnerabilities linked to pre-COVID-19 and COVID-19-related challenges.

Creating the conditions that enable people's options to safely stay where they are, to leverage the full potential benefits of dignified migration, and to avert, minimize and address displacement and related protection needs is a significant concern for both climate and human mobility policies and cooperation, especially as countries are faced with decisions to expand mobility options that have been constrained throughout the COVID-19 crisis.

---

[93] United Nations High Commissioner for Refugees and Potsdam Institute for Climate Impact Research. *COVID-19, Displacement and Climate Change*, June 2020, https://www.unhcr.org/protection/environment/5ef1ea167/covid-19-displacement-climate-change.html

[94] https://www.internal-displacement.org/expert-opinion/tropical-cyclone-harold-and-covid-19-a-double-blow-to-the-pacific-islands

[95] Millership, E., 2020: *Cyclone Harold brings new meaning to the concept of remote working in the Pacific Islands*, https://www.etcluster.org/blog/virus-and-storm, cited in International Federation of Red Cross and Red Crescent Societies: 2020, *World Disasters Report 2020*, https://media.ifrc.org/ifrc/world-disaster-report-2020/

[96] United Nations Office for the Coordination of Humanitarian Affairs, *Philippines: Typhoon Vongfong (Ambo) Snapshot (As of 20 May 2020)*, https://reliefweb.int/report/philippines/philippines-typhoon-vongfong-ambo-snapshot-20-may-2020, cited in International Federation of Red Cross and Red Crescent Societies: 2020, *World Disasters Report 2020*, https://media.ifrc.org/ifrc/world-disaster-report-2020/

[97] United Nations Office for the Coordination of Humanitarian Affairs. Asia Pacific Regional Humanitarian Update: *Typhoon Vongfong leaves trail of damage as the country grapples with the 'new normal'*, 20 May 2020, https://reports.unocha.org/en/country/asia-pacific/card/tjXV99QVBE/

[98] Department of Social Welfare and Development, Disaster Response Operations Monitoring and Information Center. *Terminal Report on Typhoon "Ambo"*, 9 July 2020, https://reliefweb.int/report/philippines/dswd-dromic-terminal-report-typhoon-ambo-09-july-2020-6pm

[99] United Nations Office for the Coordination of Humanitarian Affairs. *Humanitarian Needs Overview El Salvador, Guatemala and Honduras, Addendum: Impact of COVID-19 (May 2020)*, https://reliefweb.int/report/el-salvador/humanitarian-needs-overview-el-salvador-guatemala-and-honduras-addendum-impact

Clean energy, disaster-proof infrastructure and early warning systems

Meeting the aim of the 2015 Paris Agreement, "to strengthen the global response to the threat of climate change by keeping a global temperature rise this century well below 2 degrees Celsius above pre-industrial levels and to pursue efforts to limit the temperature increase even further to 1.5 degrees Celsius",[a] requires sizeable reductions in carbon emissions. The International Monetary Fund in the October 2020 World Economic Outlook showed that a push in green infrastructure investment combined with steadily rising carbon prices could deliver the emission reductions needed to limit the increase in temperatures and to put the global economy on a more sustainable growth path.

Climate change mitigation policies such as emission limits, emission trading programs, feed-in tariffs that provide a guaranteed price for producers of renewable energy, carbon taxes, and research and development subsidies have gradually become more popular over time (Figure 22a). The introduction of environmental policies has been accompanied by increases in global innovation and investment in clean energy technologies (Figure 22b) and has made important contributions to the reallocation of innovation, electricity generation, and employment towards low-carbon activities (Figure 22c-e).

A further green infrastructure investment push and subsidies for renewable energy generation, combined with pre-announced gradually increasing carbon prices, would lead to the emissions reductions that are needed to keep temperature increases to safer levels (Figure 22g). In turn, targeted support for poorer households and policies that facilitate job reallocation from high-carbon to low-carbon sectors would ensure a fair transition. The costs of the transition to a low-carbon global economy are manageable with green investment boosting economic activity and employment and thus compensating for some of the costs associated with carbon taxes.

While the current global recession caused by the COVID-19 pandemic can make it challenging to enact the policies needed for mitigation, it also presents opportunities to put the economy on a greener path by providing correct price signals and other financial incentives in order to boost investment in green and resilient public infrastructure, thus supporting the national economic output and employment during the recovery phase.

[a] https://unfccc.int/process-and-meetings/the-paris-agreement/the-paris-agreement

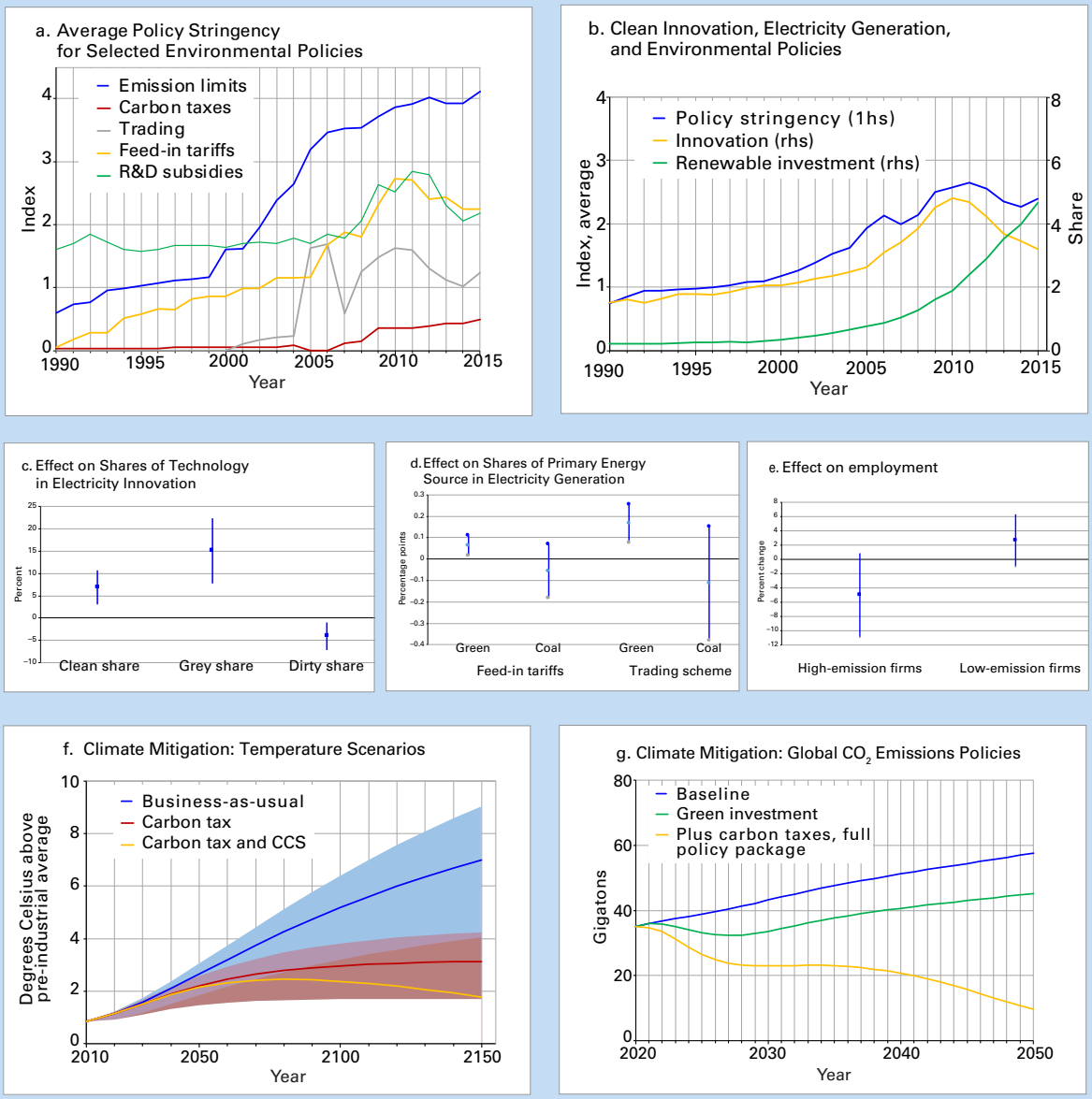

Figure 22. Impact of climate change mitigation policies. Note: In panels c, d and e, whiskers represent 90 percent confidence intervals. In panel f, the shaded areas represent high and low climate sensitivity. CCS = carbon capture and storage. See IMF (2020b) for full details.
Sources: International Monetary Fund; International Energy Agency; Organisation for Economic Co-operation and Development Environmental Policy Stringency Index; and Worldwide Patent Statistical Database

Adaptation policies aimed at enhancing resilience to a changing climate, such as investing in disaster-proof infrastructure and early warning systems, risk sharing through financial markets, and the development of social safety nets, can limit the impact of weather-related shocks and help the economy recover faster (International Monetary Fund, 2017). Adaptation strategies play a key role in countries that are particularly vulnerable to climate change, such as low-income countries located in hot regions and areas exposed to more frequent or severe natural disaster risks (Figure 23).

Cantelmo, A., et al., 2019: Macroeconomic Outcomes in Disaster-Prone Countries, *International Monetary Fund Working Paper* 19/217, https://www.imf.org/en/Publications/WP/Issues/2019/10/11/Macroeconomic-Outcomes-in-Disaster-Prone-Countries-48704.

Organisation for Economic Co-operation and Development, 2020: Environmental Policy Stringency index, https://doi.org/10.1787/2bc0bb80-en

International Monetary Fund, 2017: Seeking Sustainable Growth: Short-Term Recovery, Long-Term Challenges. Chapter 3: The Effects of Weather Shocks on Economic Activity: How Can Low-Income Countries Cope?, https://www.imf.org/en/Publications/WEO/Issues/2017/09/19/world-economic-outlook-october-2017.

International Monetary Fund, 2019: Fiscal Monitor: How to Mitigate Climate Change, https://www.imf.org/en/Publications/FM/Issues/2019/09/12/fiscal-monitor-october-2019

International Monetary Fund, 2020a: Regional Economic Outlook. Sub-Saharan Africa: COVID-19: An Unprecedented Threat to Development. Chapter 2, Adapting to Climate Change in Sub-Saharan Africa, https://www.imf.org/en/Publications/REO/SSA/Issues/2020/04/01/sreo0420

International Monetary Fund, 2020b: World Economic Outlook, A Long and Difficult Ascent. Chapter 3, Mitigating Climate Change—Growth- and Distribution-Friendly Strategies, https://www.imf.org/en/Publications/WEO/Issues/2020/09/30/world-economic-outlook-october-2020

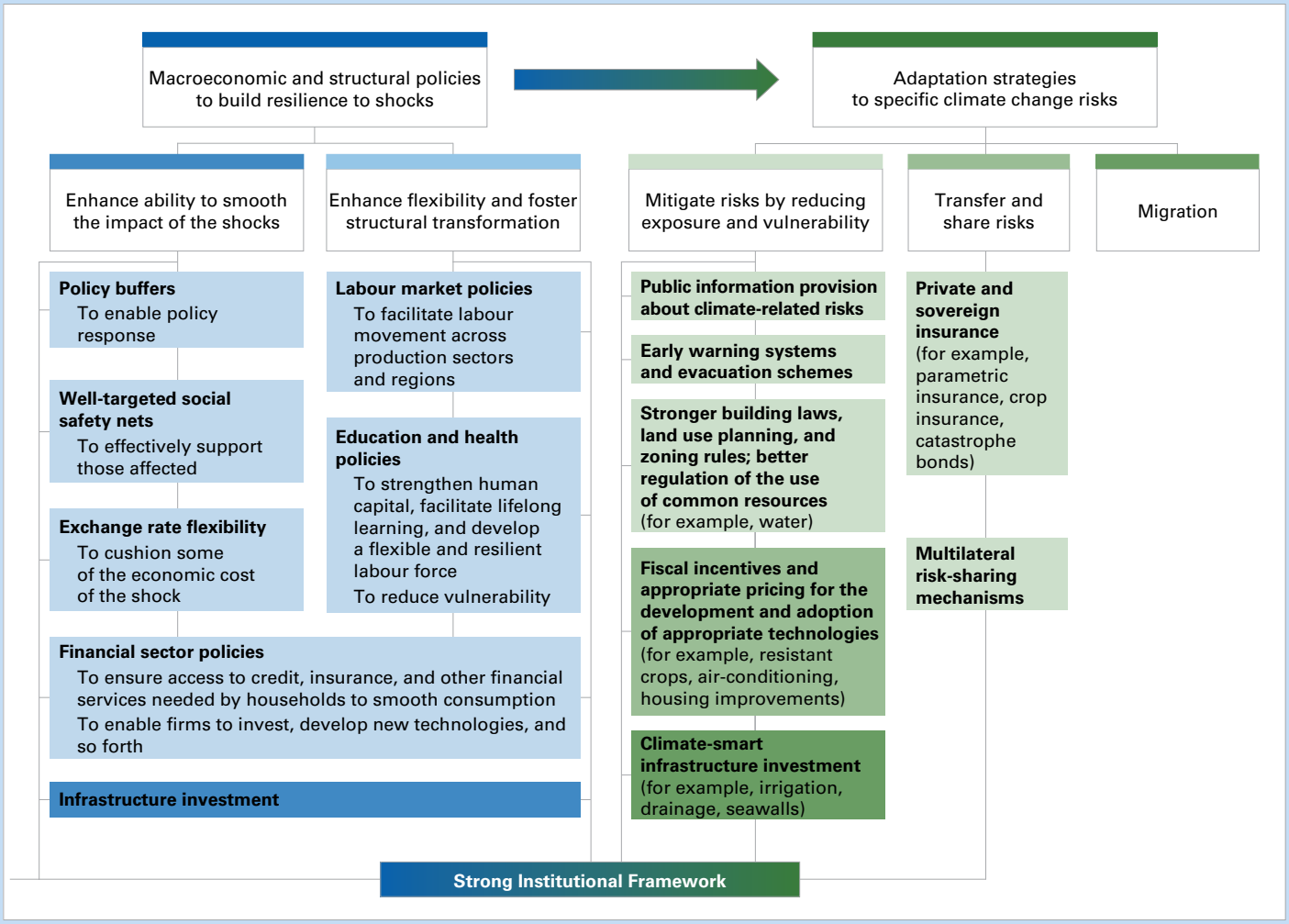

Figure 23 Climate change adaptation policies toolkit. *Source:* IMF, 2017

CASE STUDY 1: PROTECTING FARMERS IN PAKISTAN FROM THE COMPOUNDED IMPACTS OF SEVERE WEATHER, LOCUSTS AND COVID-19

Floods following heavy monsoon rains in August and September 2020 severely damaged livelihoods, causing the loss of livestock and crops across 20 districts of Sindh province in Pakistan. Concurrently, a desert locust outbreak affected 46 districts across major agricultural provinces, with breeding favoured by the unusual weather conditions. More than a third of the crop area in the region was severely affected, threatening food security and the livelihoods of farming households. COVID-19 further compounded the response to the outbreak. FAO's forecasts and tracking of locust swarms in the region, combined with local situation analysis, helped the Government of Pakistan put effective surveillance and control operations in place. As a result, Pakistan was able to survey 61.4 million hectares and treat 1.13 million hectares of cropland thereafter declared locust free.

CASE STUDY 2: FORECAST-BASED FINANCING AND ANTICIPATORY ACTION IN BANGLADESH

To reduce the impact of severe floods during the 2020 monsoon season in Bangladesh, the World Food Programme (WFP) and its partners used robust early warning data to transfer cash to vulnerable families several days before flood impacts.[a] Beneficiaries used the funds to buy food and medicine, fortify homesteads, protect critical assets, and transport livestock and vulnerable family members to safety. The aim of this endeavour was to offer more and faster support to help communities prepare and protect themselves before the next disaster. Pre-positioning of finances for these forecast-based actions was possible due to the US$ 140 million "Anticipatory Humanitarian Action" project led by the United Nations Central Emergency Response Fund (CERF).[b] Based on a weather forecast issued on 4 July 2020, which predicted severe flooding in five vulnerable districts of Bangladesh by mid-month, CERF immediately disbursed its first-ever anticipatory humanitarian funding for flood events. Out of the US$ 5.2 million disbursed in total, WFP used US$ 4.25 million to reach 145 000 people with mobile-phone-based cash transfers four days before water in the Brahmaputra River rose to dangerous levels.[c]

---

[a] World Food Programme. *Economic and food security implications of the COVID-19 outbreak*, https://docs.wfp.org/api/documents/WFP-0000113742/download/

[b] United Nations Office for the Coordination of Humanitarian Affairs. UN humanitarian chief to release up to $140M in CERF funds for anticipatory-action projects, https://reliefweb.int/report/world/un-humanitarian-chief-release-140m-cerf-funds-anticipatory-action-projects

[c] World Food Programme. *Faster than floods: WFP works to avoid a double-disaster in Banglades*h, https://insight.wfp.org/faster-than-floods-how-to-prevent-a-double-disaster-in-bangladesh-112adfd75ff0

Data set details

TEMPERATURE DATA

Global mean temperature is reported as the mean of the five data sets listed below. Global mean temperature anomalies are expressed relative to the 1850–1900 average. However, only HadCRUT5 goes back to 1850. The averages for the NOAAGlobalTemp and GISTEMP data sets are set equal to that of HadCRUT4 over the period 1880–1900 and the averages for the two reanalyses are set to equal that of HadCRUT4 over the period 1981–2010. HadCRUT4 is used as a basis for aligning other data sets for continuity with previous reports.

HadCRUT.5.0.1.0 —Morice, C.P. et al., 2021. An Updated Assessment of Near-Surface Temperature Change From 1850: The HadCRUT5 Data Set. *Journal of Geophysical Research: Atmospheres,* 126(3): e2019JD032361. doi: https://doi.org/10.1029/2019JD032361. HadCRUT.5.0.1.0 data were obtained from http://www.metoffice.gov.uk/hadobs/hadcrut5 on 14 February 2021 and are © British Crown Copyright, Met Office 2021, provided under an Open Government License, http://www.nationalarchives.gov.uk/doc/open-government-licence/version/3/.

NOAAGlobalTemp v5 — Zhang, H.-M., et al., NOAA Global Surface Temperature Dataset (NOAAGlobalTemp), Version 5.0. NOAA National Centers for Environmental Information. doi:10.7289/V5FN144H, https://www.ncei.noaa.gov/access/metadata/landing-page/bin/iso?id=gov.noaa.ncdc:C00934.

Huang, B. et al., 2020: Uncertainty Estimates for Sea Surface Temperature and Land Surface Air Temperature in NOAAGlobalTemp Version 5. *Journal of Climate* 33(4): 1351–1379, https://journals.ametsoc.org/view/journals/clim/33/4/jcli-d-19-0395.1.xml.

GISTEMP v4 — GISTEMP Team, 2019: GISS Surface Temperature Analysis (GISTEMP), version 4. NASA Goddard Institute for Space Studies, https://data.giss.nasa.gov/gistemp/.

Lenssen, N.J.L. et al., 2019: Improvements in the GISTEMP Uncertainty Model. *Journal of Geophysical Research: Atmospheres* 124(12): 6307–6326, doi: https://doi.org/10.1029/2018JD029522.

ERA5 — Hersbach, H. et al., 2020 : The ERA5 Global Reanalysis. *Quarterly Journal of the Royal Meteorological Society* 146(730): 1999–2049, doi: https://doi.org/10.1002/qj.3803.

JRA-55 — Kobayashi, S. et al., 2015: The JRA-55 Reanalysis: General Specifications and Basic Characteristics. *Journal of the Meteorological Society of Japan*. Ser. II 93(1): 5–48, doi: 10.2151/jmsj.2015-001, https://www.jstage.jst.go.jp/article/jmsj/93/1/93_2015-001/_article.

GREENHOUSE GAS DATA

Estimated concentrations from 1750 are used to represent pre-industrial conditions. Calculations assume a pre-industrial mole fraction of 278 ppm for CO_2, 722 ppb for CH_4 and 270 ppb for N_2O.

World Meteorological Organization, 2020: *WMO Greenhouse Gas Bulletin: The State of Greenhouse Gases in the Atmosphere Based on Global Observations through 2019*, No. 16, https://library.wmo.int/index.php?lvl=notice_display&id=21795#.X7v7IM1KhPY.

World Data Centre for Greenhouse Gases operated by Japan Meteorological Agency https://gaw.kishou.go.jp/

OCEAN HEAT CONTENT DATA

Cheng, L. et al., 2017: Improved Estimates of Ocean Heat Content from 1960 to 2015. *Science Advances* 3(3): e1601545, doi: 10.1126/sciadv.1601545, https://advances.sciencemag.org/content/3/3/e1601545.

CMEMS (CORA, http://marine.copernicus.eu/science-learning/ocean-monitoring-indicators)

Desbruyères, D.G. et al., 2016: Deep and Abyssal Ocean Warming from 35 Years of Repeat Hydrography. *Geophysical Research Letters* 43(19): 10,356-10,365, doi: https://doi.org/10.1002/2016GL070413.

Domingues, C.M. et al., 2008: Improved Estimates of Upper-Ocean Warming and Multi-Decadal Sea-Level Rise. *Nature* 453(7198): 1090–1093, doi: 10.1038/nature07080, https://www.nature.com/articles/nature07080.

Gaillard, F. et al., 2016: In Situ–Based Reanalysis of the Global Ocean Temperature and Salinity with ISAS: Variability of the Heat Content and Steric Height. *Journal of Climate* 29(4): 1305–1323, doi: https://journals.ametsoc.org/view/journals/clim/29/4/jcli-d-15-0028.1.xml.

Good, S.A. et al., 2013: EN4: Quality Controlled Ocean Temperature and Salinity Profiles and Monthly Objective Analyses with Uncertainty Estimates. *Journal of Geophysical Research: Oceans* 118(12): 6704–6716, doi: https://agupubs.onlinelibrary.wiley.com/doi/full/10.1002/2013JC009067.

Hosoda, S. et al., 2008: A Monthly Mean Dataset of Global Oceanic Temperature and Salinity Derived from Argo Float Observations. J*AMSTEC Report of Research and Development*, 8: 47–59, doi: https://www.jstage.jst.go.jp/article/jamstecr/8/0/8_0_47/_article.

Ishii, M. et al., 2017: Accuracy of Global Upper Ocean Heat Content Estimation Expected from Present Observational Data Sets. *Sola*, 13: 163–167, doi: https://www.jstage.jst.go.jp/article/sola/13/0/13_2017-030/_article.

IPRC, http://apdrc.soest.hawaii.edu/projects/Argo/

Levitus, S. et al., 2012: World Ocean Heat Content and Thermosteric Sea Level Change (0–2000 m), 1955–2010. *Geophysical Research Letters*, 39(10), doi: https://agupubs.onlinelibrary.wiley.com/doi/full/10.1029/2012GL051106.

Li, H. et al., 2017: Development of a Global Gridded Argo Data Set with Barnes Successive Corrections. *Journal of Geophysical Research: Oceans*, 122(2): 866–889, doi: https://doi.org/10.1002/2016JC012285.

Roemmich, D. and J. Gilson. 2009: The 2004–2008 Mean and Annual Cycle of Temperature, Salinity, and Steric Height in the Global Ocean from the Argo Program. *Progress in Oceanography*, 82(2): 81–100, doi: https://www.sciencedirect.com/science/article/abs/pii/S0079661109000160?via%3Dihub.

Roemmich, D. et al., 2015: Unabated Planetary Warming and Its Ocean Structure since 2006. *Nature Climate Change*, 5(3): 240–245. doi: https://www.nature.com/articles/nclimate2513?page=1.

von Schuckmann, K. and P.-Y. Le Traon, 2011: How Well Can We Derive Global Ocean Indicators from Argo Data? *Ocean Science*, 7(6): 783–791, doi: https://os.copernicus.org/articles/7/783/2011/.

SEA-LEVEL DATA

Archiving, Validation and Interpretation of Satellite Oceanographic data (AVISO): Legeais, J.-F. et al., 2018: An Improved and Homogeneous Altimeter Sea Level Record from the ESA Climate Change Initiative. *Earth System Science Data*, 10(1): 281–301, doi: https://essd.copernicus.org/articles/10/281/2018/.

Copernicus Marine Environment Monitoring Service (CMEMS): Pujol, M.-I. et al., 2016: DUACS DT2014: The New Multi-Mission Altimeter Data Set Reprocessed over 20 Years. *Ocean Science*, 12(5): 1067–1090. doi: https://os.copernicus.org/articles/12/1067/2016/.

Ablain, M. et al., 2017: Satellite Altimetry-Based Sea Level at Global and Regional Scales. *Surveys in Geophysics*, 38(1): 7–31. doi: https://link.springer.com/article/10.1007/s10712-016-9389-8.

Escudier, P. A. et al., 2017: Satellite radar altimetry: principle, accuracy and precision. In Satellite Altimetry Over Oceans and Land Surfaces (D. Stammer and A. Cazenave, eds).

MARINE HEATWAVE DATA

MHWs are categorized as moderate when the sea-surface temperature (SST) is above the 90th percentile of the climatological distribution for five days or longer; the subsequent categories are defined with respect to the difference between the SST and the climatological distribution average: strong, severe, or extreme, if that difference is, respectively, more than two, three or four times the difference between the 90th percentile and the climatological distribution average (Hobday et al., 2018).

The baseline used for MHWs is 1982–2011, which is shifted by one year from the standard normal period of 1981–2010 because the satellite SST series on which it is based starts in 1981.

Hobday, A.J. et al., 2018: Categorizing and Naming Marine Heatwaves. *Oceanography,* 31(2): 1–13. doi: https://eprints.utas.edu.au/27875/.

NOAA OISST v2: Optimum Interpolation Sea Surface Temperature (OISST):
Banzon, V. et al., 2016: A Long-Term Record of Blended Satellite and in Situ Sea-Surface Temperature for Climate Monitoring, Modeling and Environmental Studies. *Earth System Science Data*, 8(1): 165–176. doi: https://essd.copernicus.org/articles/8/165/2016/.

OCEAN ACIDIFICATION DATA

Data from sampling sites were extracted from the 14.3.1 data portal (http://oa.iode.org) for the time period from 1 January 2010 to 8 January 2020. Annual averages, maximums and minimums were calculated for each station for each year.

The global pH data set is based on a variety of oceanographic variables from Copernicus Marine Service (CMEMS):
https://resources.marine.copernicus.eu/?option=com_csw&view=details&product_id=GLOBAL_OMI_HEALTH_carbon_ph_area_averaged

SEA-ICE DATA

Data set background:
The sea ice section uses data from the EUMETSAT OSI SAF Sea Ice Index v2.1 (OSI-SAF, based on Lavergne et al., 2019) and the NSIDC v3 Sea Ice Index (Fetterer et al., 2017). Sea-ice concentrations are estimated from microwave radiances measured from satellites. Sea-ice extent is calculated as the area of ocean grid cells where the sea-ice concentration exceeds 15%. Although there are relatively large differences in the absolute extent between data sets, the data sets have good agreement on the year-to-year changes and the trends. In this report, NSIDC data are reported for absolute extents (for example, "18.95 million km^2") for consistency with earlier reports, while rankings are reported for both data sets.

Fetterer, F., K. Knowles, W. N. Meier, M. Savoie and A. K. Windnagel. 2017, updated daily. Sea Ice Index, Version 3. Boulder, Colorado USA. NSIDC: National Snow and Ice Data Center. doi: https://nsidc.org/data/G02135/versions/3.

EUMETSAT Ocean and Sea Ice Satellite Application Facility, Sea-ice index 1979-onwards (v2.1, 2020), OSI-420, Data extracted from OSI SAF FTP server: 1979–2020, northern and southern hemisphere.

Lavergne, T. et al., 2019: Version 2 of the EUMETSAT OSI SAF and ESA CCI Sea-Ice Concentration Climate Data Records. *The Cryosphere*, 13(1): 49–78, doi: https://tc.copernicus.org/articles/13/49/2019/.

GREENLAND ICE SHEET DATA

Data are from the Polar Portal http://polarportal.dk/en/home/.

The ice discharge series has been available since 1986 and is derived from satellite data which can be used to measure glacier flow speeds all around the edges. These data are used to estimate how much ice is being lost as icebergs.

Slightly different models have been used to calculate the SMB over time. These models, using different forcing data, may give slightly different results.

ANTARCTIC ICE SHEET DATA

Data shown are from:
Velicogna, I. et al., 2020: Continuity of Ice Sheet Mass Loss in Greenland and Antarctica From the GRACE and GRACE Follow-On Missions. *Geophysical Research Letters*, 47(8): e2020GL087291, doi: https://agupubs.onlinelibrary.wiley.com/doi/abs/10.1029/2020GL087291.

GLACIERS

Information on glaciers is from the World Glacier Monitoring Service https://wgms.ch/.

WGMS (2020, updated, and earlier reports). *Global Glacier Change Bulletin* No. 3 (2016–2017). Zemp, M., Gärtner-Roer, I., Nussbaumer, S. U., Bannwart, J., Rastner, P., Paul, F., and Hoelzle, M. (eds.), ISC(WDS)/IUGG(IACS)/UNEP/UNESCO/WMO, World Glacier Monitoring Service, Zurich, Switzerland, 274 pp., publication based on database version: doi: https://wgms.ch/data_databaseversions/.

PRECIPITATION DATA

The following GPCC data sets were used in the analysis:

- First Guess Monthly, doi: 10.5676/DWD_GPCC/FG_M_100, https://opendata.dwd.de/climate_environment/GPCC/html/gpcc_firstguess_doi_download.html

- Monitoring Product (Version 6), doi: 10.5676/DWD_GPCC/MP_M_V6_100 https://opendata.dwd.de/climate_environment/GPCC/html/gpcc_monitoring_v6_doi_download.html

- Full Data Monthly (Version 2018), doi: 10.5676/DWD_GPCC/FD_M_V2018_100 https://opendata.dwd.de/climate_environment/GPCC/html/fulldata-monthly_v2018_doi_download.html

- First Guess Daily, doi: 10.5676/DWD_GPCC/FG_D_100 https://opendata.dwd.de/climate_environment/GPCC/html/gpcc_firstguess_daily_doi_download.html

- Full Data Daily (Version 2018), doi: 10.5676/DWD_GPCC/FD_D_V2018_100 https://opendata.dwd.de/climate_environment/GPCC/html/fulldata-daily_v2018_doi_download.html

The normal period used in the precipitation maps is 1951–2010. A longer reference period is used because precipitation is more variable than temperature, so a longer averaging period is needed in order to obtain a reliable average. This is particularly important in arid regions, where precipitation is intermittent.

For extreme precipitation indices, the period 1982–2016 is used as this is the period covered by the full GPCC daily data set (version 2018). As for assessing changes in annual precipitation, a longer baseline allows for a more reliable estimate of the thresholds and averages on which the extremes indices are based.

ARCTIC SIDEBAR DATA

The Arctic sidebar data is based on data from other sections within this report, on information from regional and country reports, as well as on the following data sets:

Copernicus Climate Change Service (C3S) ERA5 temperature dataset. Described in Hersbach, H, Bell, B, Berrisford, P, et al. The ERA5 global reanalysis. Q J R Meteorol Soc. 2020; 146: 1999– 2049. https://doi.org/10.1002/qj.3803, available at: https://cds.climate.copernicus.eu/cdsapp#!/dataset/ecv-for-climate-change?tab=overview.

CAMS wildfire emission data set and interpretation thereof https://atmosphere.copernicus.eu/copernicus-reveals-summer-2020s-arctic- wildfires-set-new-emission-records#

Copernicus Atmosphere Monitoring Service Global Fire Assimilation System (GFAS) https://confluence.ecmwf.int/display/CKB/CAMS%3A+Global+Fire+Assimilation+System+%28GFAS%29+data+documentation

CAMS wildfire emission data set and interpretation thereof: https://atmosphere.copernicus.eu/copernicus-reveals-summer-2020s-arctic-wildfires-set-new-emission-records#

List of contributors

WMO MEMBER CONTRIBUTIONS

Algeria, Argentina, Armenia, Austria, Bahrain, Belarus, Bosnia and Herzegovina, Brazil, Bulgaria, Burkina Faso, Cameroon, Canada, Chile, China, Colombia, Congo, Costa Rica, Côte d'Ivoire, Croatia, Cyprus, Czech Republic, Denmark, Estonia, Finland, France, Georgia, Germany, Greece, Guatemala, Hong Kong, China; India, Indonesia, Ireland, Israel, Italy, Japan, Jordan, Kazakhstan, Latvia, Libya, Lithuania, Luxembourg, Mali, Mauritius, Moldova, Morocco, Netherlands, New Zealand, Nigeria, Northern Macedonia, Norway, Pakistan, Paraguay, Peru, Poland, Republic of Korea, Romania, Russia, Saudi Arabia, Senegal, Serbia, Singapore, Slovakia, Slovenia, South Africa, Spain, Sudan, Sweden, Switzerland, Tunisia, Turkey, Ukraine, United Kingdom, USA, Uzbekistan, WMO Regional Association VI Regional Climate Centre (RCC)

CONTRIBUTING DATA CENTRES AND INSTITUTIONS

Global Precipitation Climatology Centre (GPCC), Deutscher Wetterdienst (DWD), Germany; National Oceanic and Atmospheric Administration (NOAA), National Centers for Environmental Information (NCEI), Pacific Marine Environmental Laboratory (PMEL), USA; National Aeronautics and Space Administration (NASA) Goddard Institute of Space Studies (GISS), USA; National Snow and Ice Data Centre (NSIDC), USA; MET Norway; Institute of Atmospheric Physics (IAP), Chinese Academy of Sciences; Center for Ocean Mega-Science, Chinese Academy of Sciences; Scientific Committee on Antarctic Research (SCAR), UK; National Isotope Centre, GNS Science, New Zealand; National Oceanographic Centre (NOC), UK; ARC Centre of Excellence for Climate Extremes, University of Tasmania, Australia; Max-Planck Institute for Biogeochemistry, Germany; Met Office, UK; University of California, USA; British Antarctic Survey (BAS), UK; ETH Zürich (ETHZ), Switzerland; Copernicus Climate Change Service (C3S); Copernicus Marine and Environment Monitoring Service (CMEMS); Copernicus Atmosphere Monitoring Service (CAMS); European Organisation for the Exploitation of Meteorological Satellites (EUMETSAT) Ocean and Sea Ice Satellite Application Facility (OSI SAF); Polar Portal, Denmark; University of Wollongong, Australia; SRON, Netherlands Institute for Space Research; Department of Atmosphere, Ocean and Earth System Modeling Research, Meteorological Research Institute, Japan; Commonwealth Scientific and Industrial Research Organisation (CSIRO), Australia; Korea Meteorological Administration (KMA), Republic of Korea; International Space Science Institute, Switzerland; Scripps Institution of Oceanography, UCSD, San Diego, USA; Japan Meteorological Agency (JMA), Japan; GRID Arendal, Norway; World Climate Research Programme (WCRP); Danmarks Meteorologiske Institut (DMI), Denmark; Bureau of Meteorology, Australia; European Centre for Medium Range Weather Forecasts, UK; Integrated Carbon Observing System (ICOS) Carbon Portal, Sweden; Woods Hole Oceanographic Institution, Massachusetts, USA; Centre National d'Études Spatiales, CNES, France; Mercator Ocean international, France; Observatoire Midi-Pyrénées, France; IFREMER, France; University of Brest, France; Centre National de la Recherche Scientifique, (CNRS), France; Institut de Recherche pour le Développement (IRD), France; Laboratoire d'Océanographie Physique et Spatiale (LOPS), France; Laboratoire d'Etudes en Géophysique et Océanographie Spatiales (LEGOS), France; Institut Universitaire Européen de la Mer (IUEM), France; CELAD, France; Sorbonne Université, France; Laboratoire d'Océanographie de Villefranche, France; World Glacier Monitoring Service (WGMS); WMO Global Cryosphere Watch; WMO Global Atmosphere Watch

UNITED NATIONS AGENCIES

United Nations Environment Programme (UNEP), World Health Organization (WHO); Food and Agriculture Organization (FAO); United Nations High Commissioner for Refugees (UNHCR); International Organization for Migration (IOM); World Food Programme (WFP); International Oceanographic Commission – United Nations (IOC-UNESCO), International Monetary Fund (IMF)

INDIVIDUAL CONTRIBUTORS

Signe Aaboe (MET Norway), Jonathan Abrahams (WHO), Jorge Alvar-Beltrán (FAO), Jana Birner (UNHCR), Jessica Blunden (NOAA NCEI), Tim Boyer (NOAA's National Centers for Environmental Information), Anny Cazenave (LEGOS CNES and OMP, France), Lijing Cheng (IAP, Chinese Academy of Sciences, China; and Center for Ocean Mega-Science, Chinese Academy of Sciences), Jocelyn Christine Turnbull (National Isotope Centre, GNS Science, New Zealand), Andrew Crotwell (NOAA, USA), Damien Desbruyères (IFREMER, University of Brest, CNRS, IRD, LOPS, France), Catia Domingues (NOC, UK; and ARC Centre of Excellence for Climate Extremes, University of Tasmania, Australia), Edward Dlugokencky (NOAA, USA), Simon Eggleston (WMO), Christoph Gerbig (Max-Planck Institute for Biogeochemistry, Germany), John Gilson (University of California, USA), Yvan Gouzenes (LEGOS and OMP, France), Luke Gregor (ETHZ), David Griffith (University of Wollongong, Australia), Lorenzo Guadagno (IOM), Brad Hall (NOAA, USA), Valentine Haran (Visiting Scientist at WMO, University of Geneva), Ana Heureux (FAO), Sander Houweling (SRON, Netherlands), Matthias Huss (ETHZ), Aamer Irshad (FAO), Masayoshi Ishii (Department of Atmosphere, Ocean and Earth System Modeling Research, Meteorological Research Institute, Japan), Kirsten Isensee (IOC UNESCO), Gregory C. Johnson (NOAA PMEL, USA), Armin Jordan (Max-Planck Institute for Biogeochemistry, Germany), Maarten Kappelle (UNEP), John Kennedy (Met Office, UK), Rachel Killick (Met Office, UK), Brian A. King (NOC, UK), Nicolas Kolodziejczyk (University of Brest, CNRS, IRD, IFREMER, LOPS, IUEM, France), Paul Krummel (CSIRO, Australia), Thomas Lavergne (MET Norway), Haeyoung Lee (KMA, Republic of Korea), Zoë Miranda Loh (CSIRO, Australia), John Lyman (NOAA PMEL, USA), Nicholas Middleton (UNEP), Maeva Monier (CELAD/Mercator Ocean International, France), Rodica Nitu (WMO/GCW), Didier Paolo Monselesan (CSIRO Oceans and Atmosphere, Hobart, Tasmania, Australia), Lorena Moreira (International Space Science Institute, Bern), Lev Neretin (FAO), Stoyka Netcheva (WMO Secretariat, Science and Innovation Department), Anne Olhoff (UNEP-DTU Partnership UDP), Giorgia Pergolini (WFP), Hamish D. Pritchard (SCAR, BAS), Evgenia Pugacheva (IMF), Claire Ransom (Visiting Scientist at WMO, Institut de Hautes Etudes Internationales et du Development), Dean Roemmich (Scripps Institution of Oceanography, UCSD, San Diego, CA, USA), Yousuke Sawa (JMA, Japan), Robert W. Schlegel (Sorbonne Université, CNRS, Laboratoire d'Océanographie de Villefranche), Tina Schoolmeester (GRID Arendal), Katherina Schoo (IOC UNESCO), Ria Sen (WFP), Joy Shumake-Guillemot (WMO/WHO), Michael Sparrow (WCRP/WMO), Martin Stendel (DMI), Faisal Syed (FAO), Oksana Tarasova (WMO Secretariat), Blair Trewin (IPCC AR6 lead author, Bureau of Meteorology, Australia), John Turner (SCAR, BAS), Freja Vamborg (ECMWF), Alex Vermuelen (ICOS Carbon Portal, Sweden), Karina von Schuckmann (Mercator Ocean international, France), Ying Wang (UNEP), Ray Weiss (Scripps Institution of Oceanography, USA), Susan E. Wijffels (CSIRO Oceans and Atmosphere, Hobart, Tasmania, Australia and Woods Hole Oceanographic Institution, USA), Michelle Yonetani (UNHCR), Markus Ziese (Deutscher Wetterdienst, Germany)

For more information, please contact:

World Meteorological Organization

7 bis, avenue de la Paix – P.O. Box 2300 – CH 1211 Geneva 2 – Switzerland

Strategic Communications Office
Cabinet Office of the Secretary-General

Tel: +41 (0) 22 730 83 14 – Fax: +41 (0) 22 730 80 27

Email: communications@wmo.int

public.wmo.int

JN 21259